REPORT NO.
UC SESM 75-3

STRUCTURES AND MATERIALS RESEARCH
DEPARTMENT OF CIVIL ENGINEERING

FINITE ELEMENT FORMULATION AND SOLUTION OF CONTACT-IMPACT PROBLEMS IN CONTINUUM MECHANICS-II

by

THOMAS J. HUGHES
ROBERT L. TAYLOR
JEROME L. SACKMAN

JANUARY 1975

STRUCTURAL ENGINEERING LABORATORY
UNIVERSITY OF CALIFORNIA
BERKELEY CALIFORNIA

Structures and Materials Research
Department of Civil Engineering

Report No. 75-3

FINITE ELEMENT FORMULATION AND SOLUTION OF CONTACT AND IMPACT PROBLEMS IN CONTINUUM MECHANICS -II

by

Thomas J. Hughes
Robert L. Taylor
Jerome L. Sackman

This report was prepared under subcontract number
N62399-73-C-0023

sponsored by

Civil Engineering Laboratory
Naval Construction Battalion Center
Port Hueneme, California

as part of NHTSA Interagency Agreement Number
DOT-HS-289-3-550 IA

Funded by National Highway Traffic
Safety Administration

Department of Transportation

January 1975

TABLE OF CONTENTS

ACKNOWLEDGEMENT

This report was prepared under Subcontract No. N62399-73-C-0023; sponsored by Civil Engineering Laboratory, Naval Construction Battalion Center, Port Hueneme, California as part of NHTSA interagency agreement No. DOT-HS-289-3-550 IA which was funded by the National Highway Traffic Safety Administration, Department of Transportation.

The opinions, findings and conclusions expressed in this publication are those of the authors and not necessarily those of the Civil Engineering Laboratory or the National Highway Traffic Safety Administration.

The authors would like to acknowledge the considerable contributions of Research Assistants Alain Curnier and Worsak Kanoknukulchai to the work reported upon herein.

INTRODUCTION

In this report we are concerned with three tasks funded under the increased effort phase of Contract No. N62399-73-C-0023 (proposal UCB-Eng-3853). The work under each task has been completed and is reported upon in Sections I to III.

Section I deals with the solutions of several Hertzian contact/impact problems obtained by the computer program FEAP. These problems demonstrate the veracity of the algorithm for Hertzian contact/impact and the importance of the impact/release conditions which are used in the program.

In Section II, a methodology for incorporating the full kinematically nonlinear contact/impact problem into a finite element computer program is initiated. The scheme developed is a logical generalization of the one used for Hertzian contact/impact.

Finally, in Section III we report upon the principal task undertaken in the increased effort phase of the contract; namely, the implementation of substructuring concepts into FEAP to increase the efficiency of the Hertzian contact/impact algorithm. The result of this work is a dramatic decrease in expended computer time for the main computational steps in the Hertzian contact/impact algorithm.

I. Numerical Results of Hertzian Contact/Impact Problems Solved by FEAP

1. Hertz Contact Problem

The Hertz static contact problem was solved and we were able to accurately compute both the contact region and the pressures over a wide range of loading. These results were presented orally to the NHTSA and were described in a progress report. The mesh is depicted in Fig. I-1 and contact pressure versus contact radius results are plotted in Fig. I-2. Data consists of:

$E = 1000.$ (Young's modulus)

$\nu = .3$ (Poisson's ratio)

$R = 8.$ (Radius of quarter sphere)

The total applied force is distributed uniformly across the top surface. The results clearly indicate that the contact pressures are given more accurately by the nodal contact forces than by the element stresses, as one might surmise they would be.

2. Impact of an Elastic Sphere Against a Rigid Wall

We have been interested in the problem of the impact of an elastic sphere against a frictionless rigid wall for several reasons. First of all it is an impact problem with a nontrivial contact area development. Secondly, the sphere geometrically approximates the shape of a head. Thirdly, it is one of the few three-dimensional impact problems for which there exists any analytical information.*

For these reasons it seemed an appropriate initial test problem for our algorithm. We have solved the problem for various meshes

*Hertz obtained a quasi-static approximate solution to this problem (see,e.g., [3]).

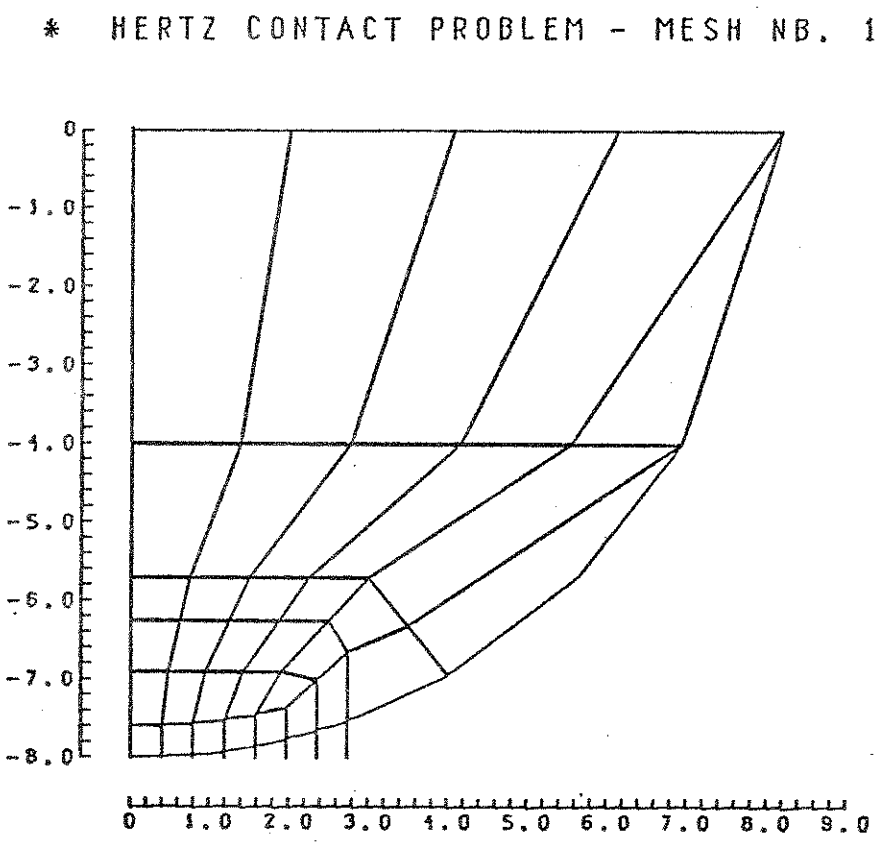
* HERTZ CONTACT PROBLEM - MESH NB. 1 *
0
-1.0
-2.0
-3.0
-4.0
-5.0
-6.0
-7.0
-8.0
0 1.0 2.0 3.0 4.0 5.0 6.0 7.0 8.0 9.0

Figure I-1

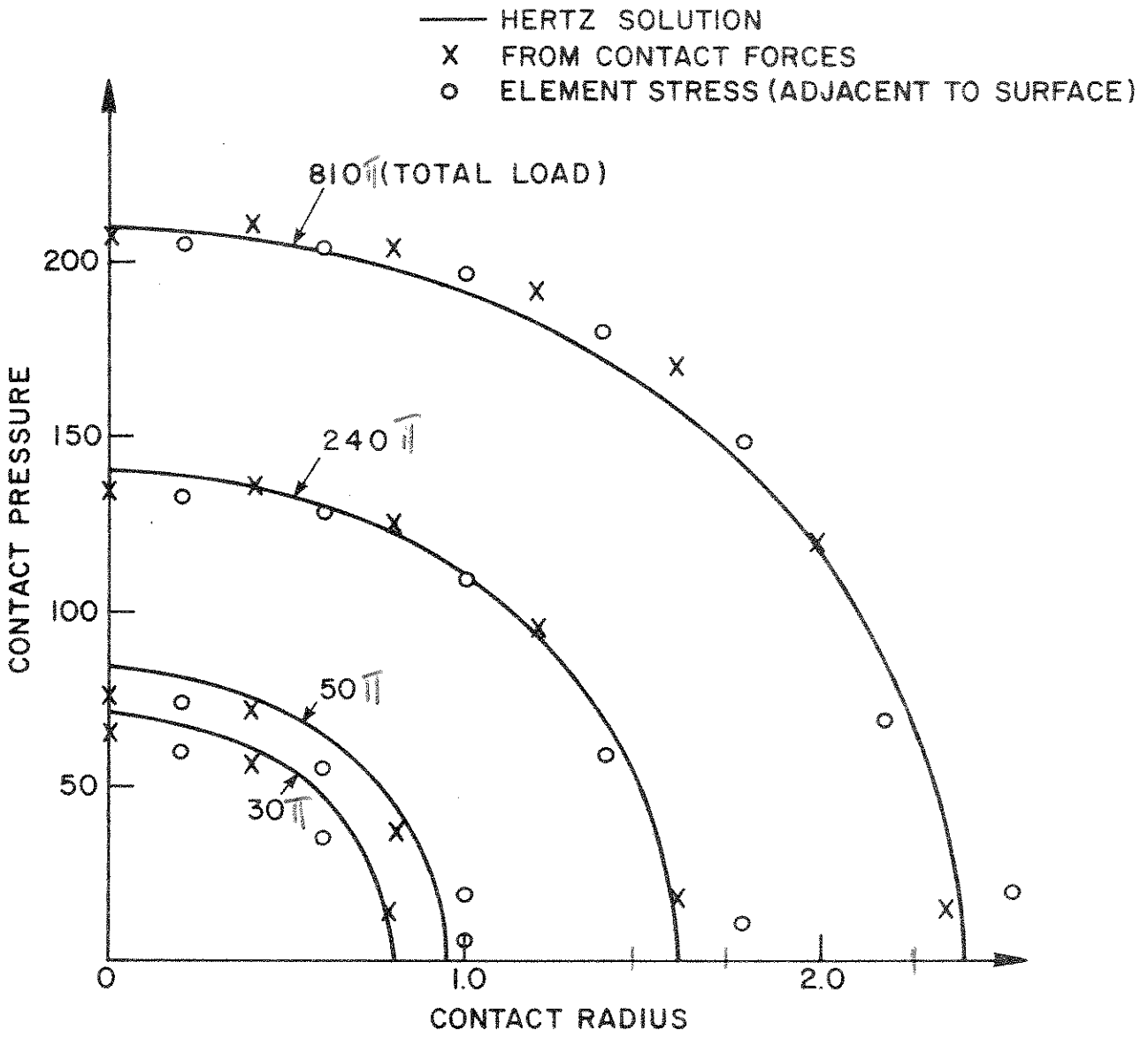
HERTZ SOLUTION
FROM CONTACT FORCES
ELEMENT STRESS (ADJACENT TO SURFACE)
810 π (TOTAL LOAD)
240 π
50 π
30 π
CONTACT PRESSURE
200
150
100
50
0
1.0
2.0
CONTACT RADIUS

FIGURE I-2

with different degrees of refinement in the contact area and over a range of impact velocities (some of these results have been previously forwarded to CEL). We note that greater impact velocities result in greater contact area. Thus one cannot normalize our computed results on the basis of initial velocity of the sphere. This is to be expected as this is a bona fide nonlinear problem (despite the fact that the body is governed by linear elasticity theory).

We include here results of two recently studied meshes, Figs. I-3 and I-4. Mesh 5 (Fig. I-3) is a rather uniform mesh with a crude contact area description, i.e., only two candidate contact nodes. Mesh 4 (Fig. I-4) is identical to Mesh 5 except in the neighborhood of the contact area which is refined to accomodate four candidate contact nodes. The computer plot of the mesh gets rather cramped in this vicinity so we have blown it up in Fig. I-5. The data for this problem is:

ρ	=	.01	(Density)
E	=	1000.	(Young's modulus)
ν	=	.3	(Poisson's ratio)
R	=	5.	(Radius of sphere)
Δt	=	.01	(Time step)

Some results for uniform initial velocities V =-.8 and -3.0, (i.e., pointing downward), are presented in Figs. I-6 through I-11. In the figure captions, Z refers to the vertical direction, thus SIGMA Z means the normal stress in the vertical direction, and TAU indicates the contact force per radian at the indicated candidate contact node (referred to as ELM 45, etc.).

IMPACT OF SPHERE, HOMOGENOUS MESH 5

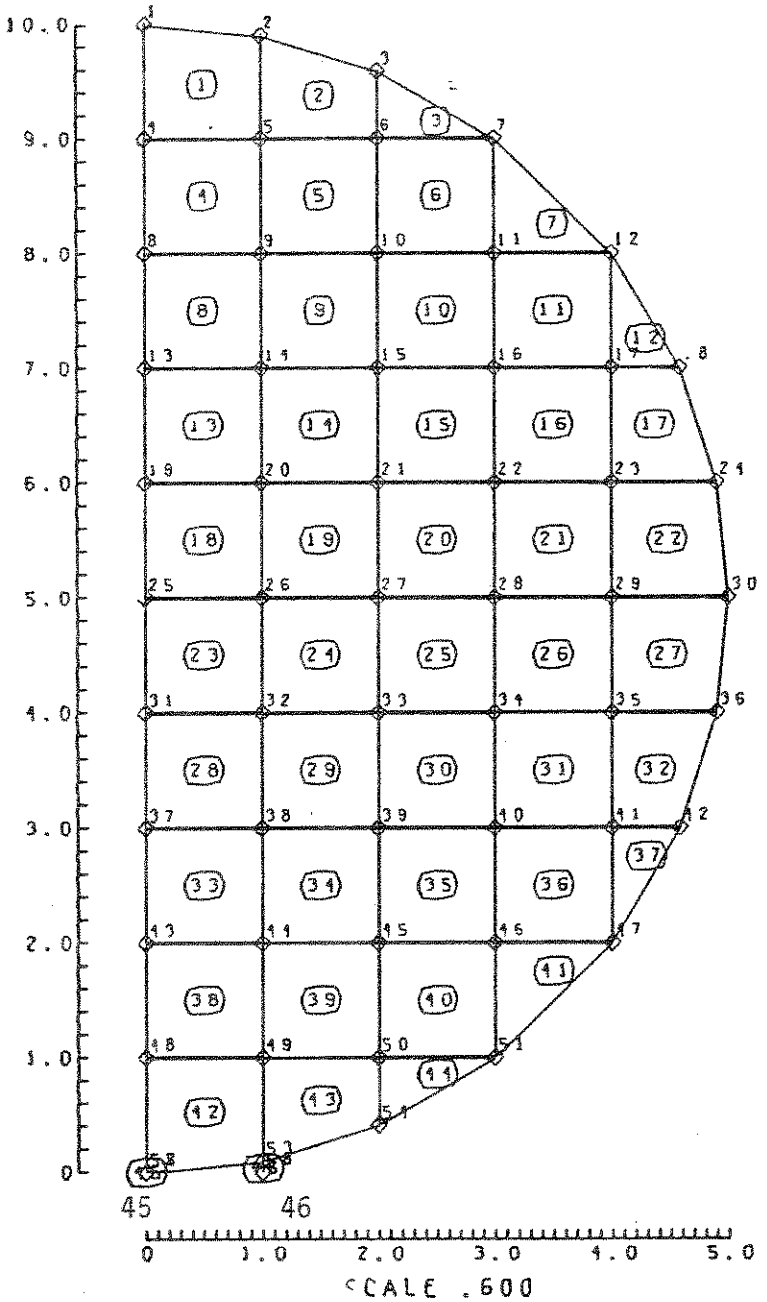

Figure I-3

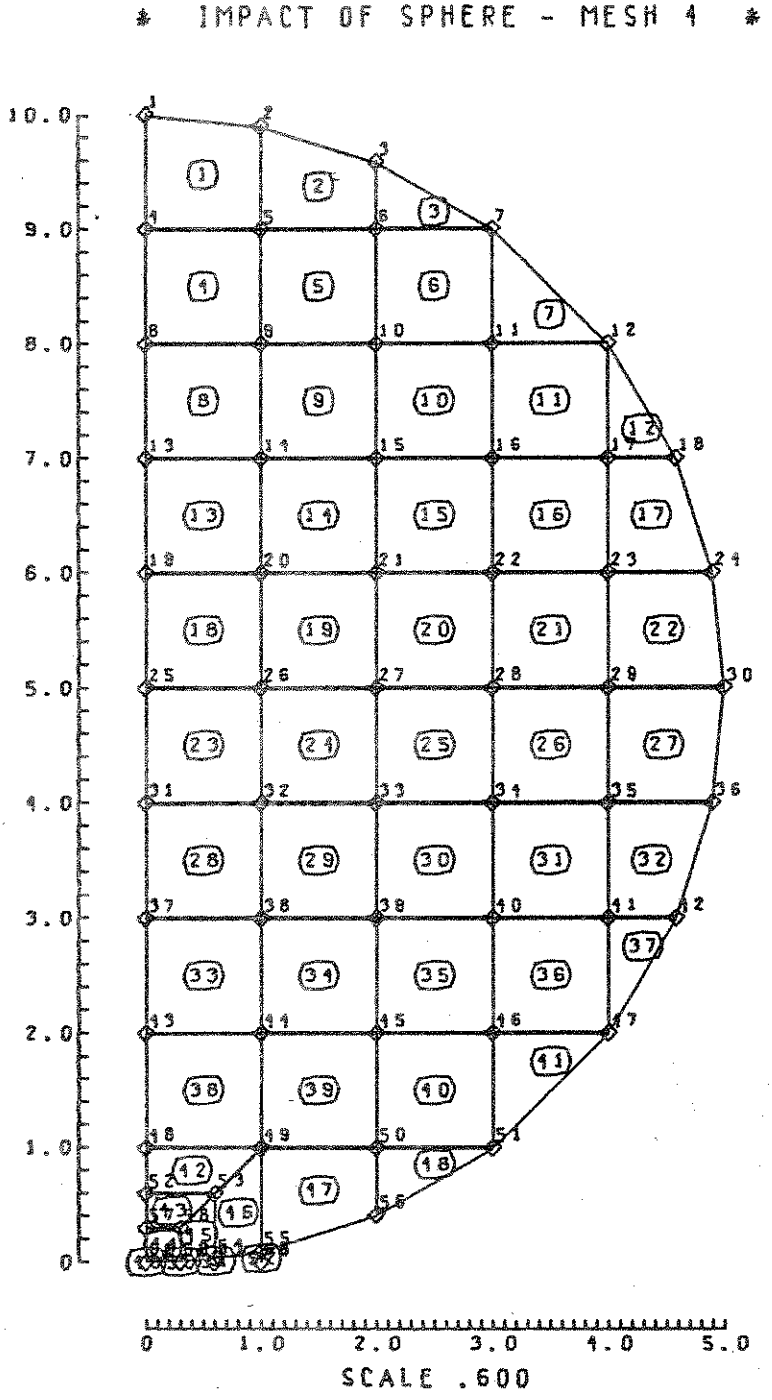
* IMPACT OF SPHERE - MESH 4 *
10.0
9.0
8.0
7.0
6.0
5.0
4.0
3.0
2.0
1.0
0
0
1.0
2.0
3.0
4.0
5.0
SCALE .600

Figure I-4

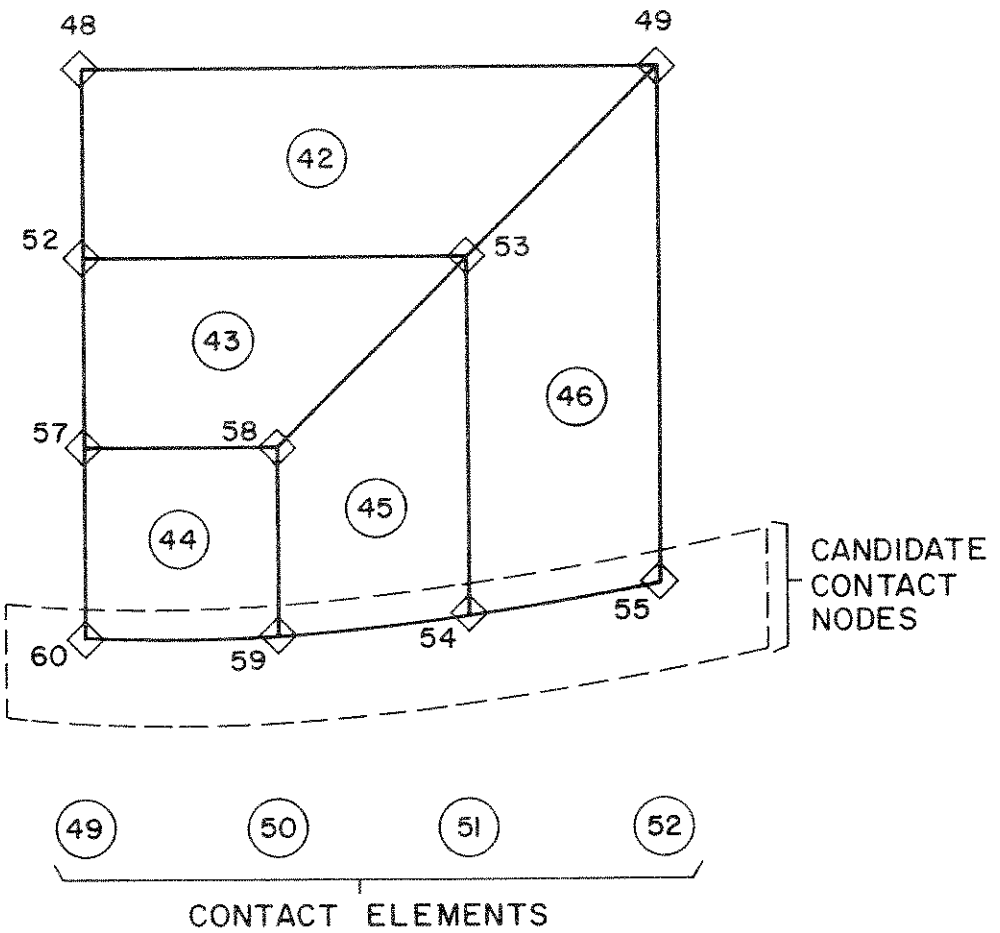

FIGURE I-5 DETAIL OF MESH 4 IN THE VICINITY OF THE CONTACT AREA.

EVOLUTION OF SOLUTIONS WITH TIME

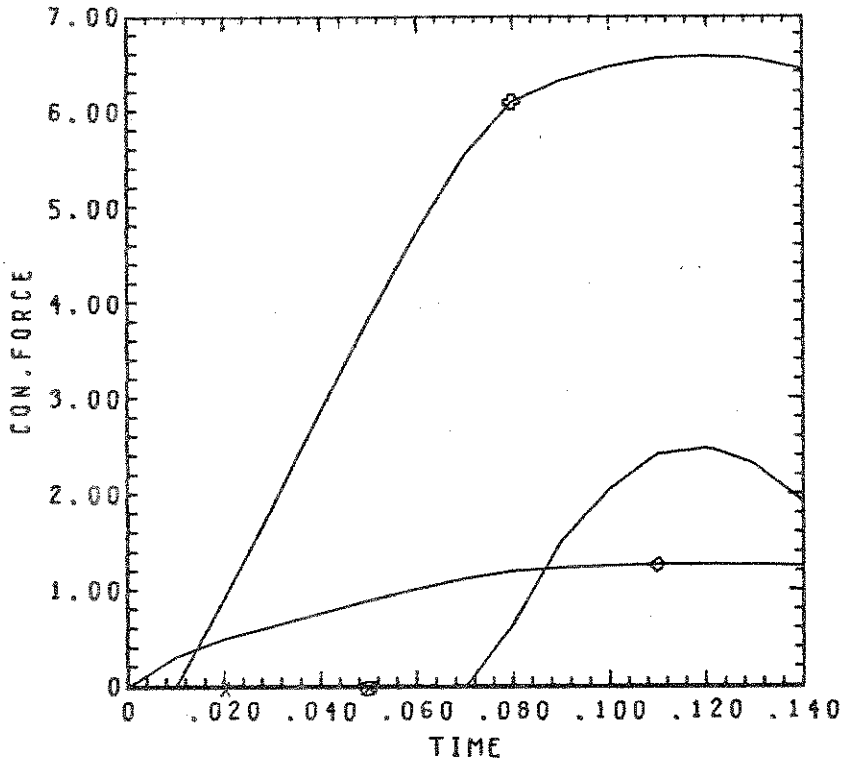

Figure I-6

EVOLUTION OF SOLUTIONS WITH TIME

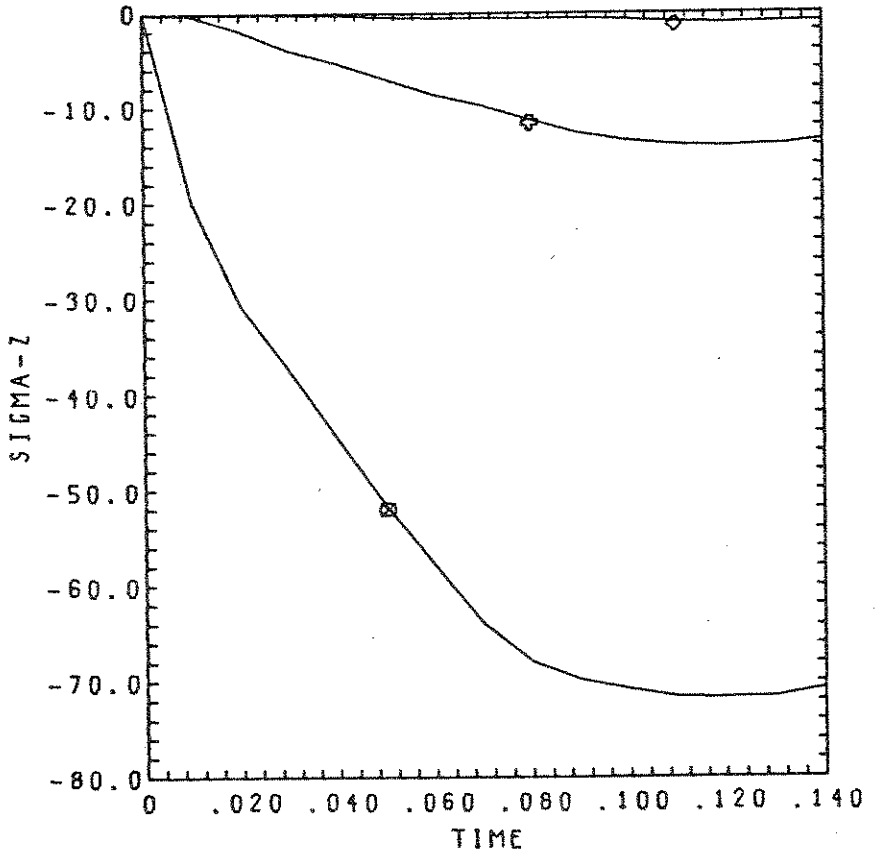

◇ - ELM. 18 SIGMA-Z ZZ- COORDS .21 5.79
◇ - 38 SIGMA-Z ZZ- .21 1.79
⊗ - 44 SIGMA-Z ZZ- .06 .24

MESH 4 V = -.8

Figure I-7

EVOLUTION OF SOLUTIONS WITH TIME

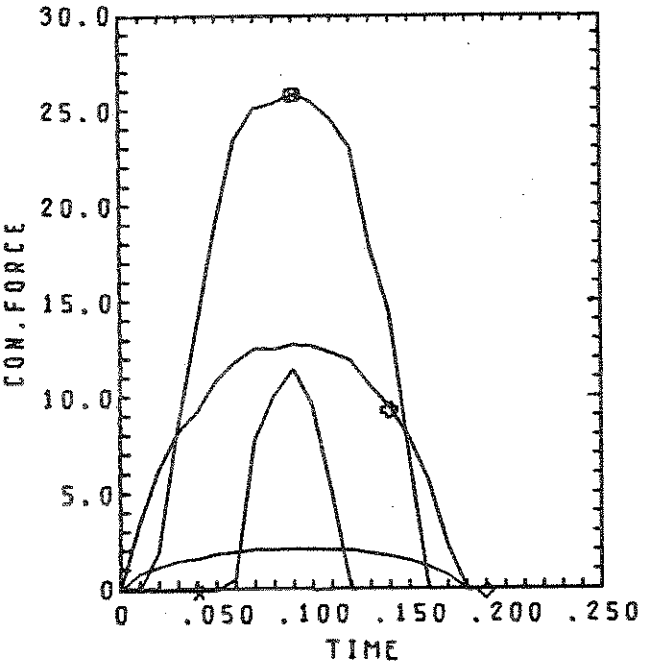

◇ - ELM. 49 CON.FORCE TAU COORDS .00 .00
⌬ - 50 CON.FORCE TAU .30 .00
⊗ - 51 CON.FORCE TAU .60 .00
✳ - 52 CON.FORCE TAU 1.00 .00

MESH 4 V = -3.

Figure I-8

EVOLUTION OF SOLUTIONS WITH TIME

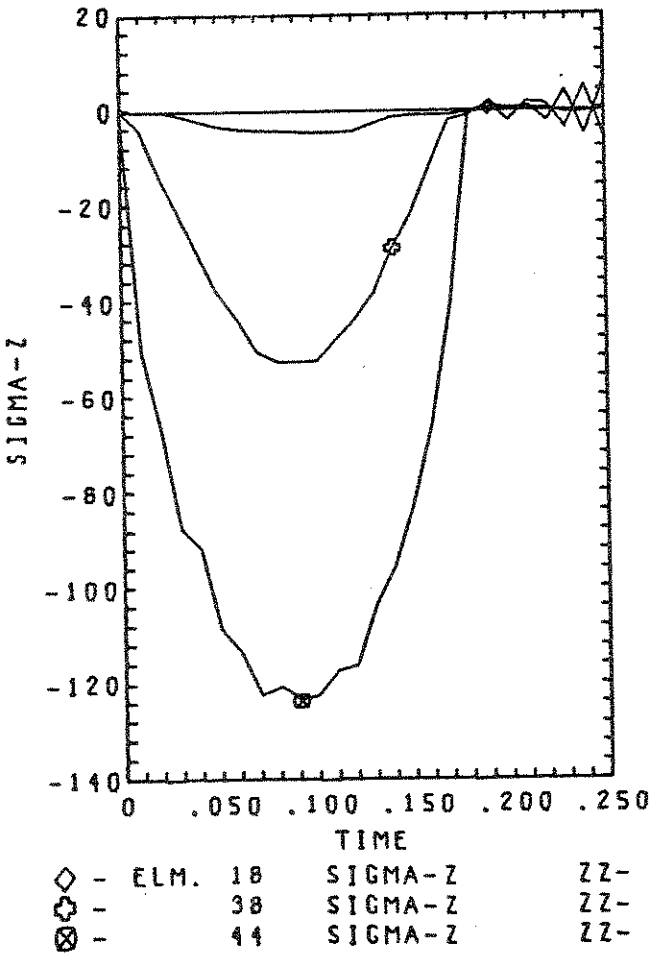

MESH 4 V = -3.

Figure I-9

EVOLUTION OF SOLUTIONS WITH TIME

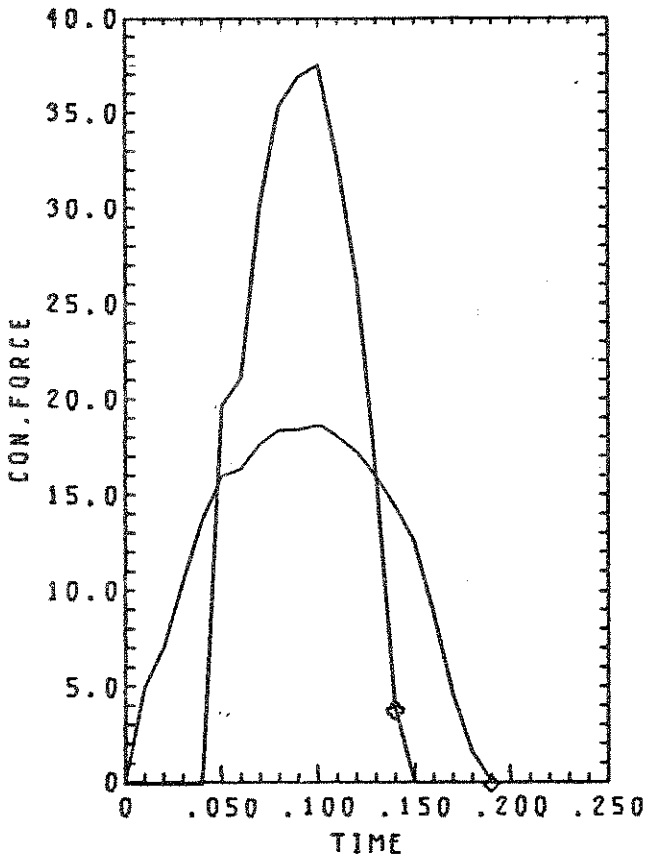

MESH 5 V = -3.

Figure I-10

EVOLUTION OF SOLUTIONS WITH TIME

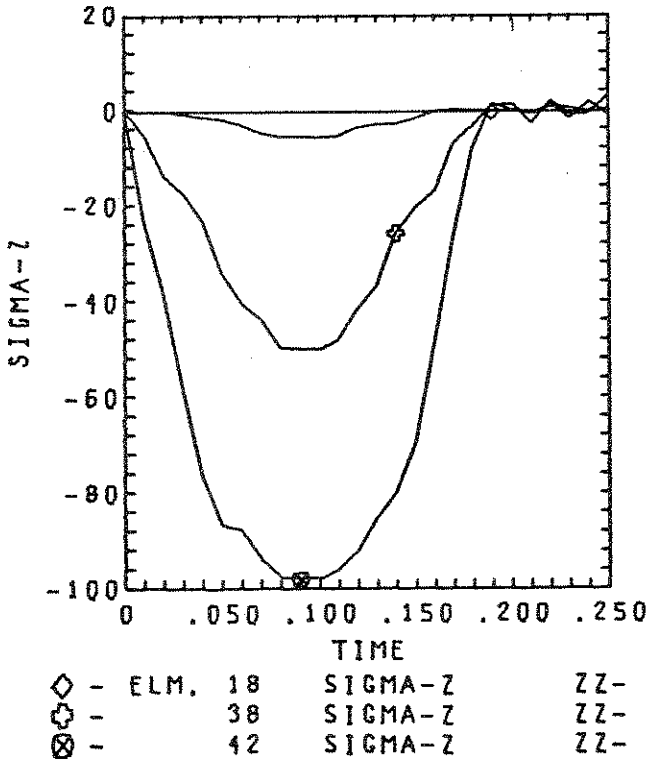

Figure I-11

The refined Mesh 4, provides smoother results than Mesh 5, as is to be expected. However, the bulk response is in good agreement. This indicates that if one is only interested in bulk properties, (e.g., total forces, release time, etc.), a rather crude description of the contact surface will suffice. One can evidently exploit this fact to economic advantage under the appropriate circumstances.

We have noted that our results, for different meshes and time steps, are quite consistent. This indicates that the results may be considered, for practical purposes, converged. Comparison with bulk properties of the approximate solution obtained by Hertz lends additional credence to this conclusion, e.g., total force and release times are within 11% (see Table I-1).

A nonlinear problem of this size (i.e., 111 degrees of freedom, 25 time steps, postprocessing for 7 plots, etc.) is currently costing us in the neighborhood of 13 dollars on the University of California's CDC 6400 computer and utilizes about 114 CPU seconds.

3. Impact of Two Elastic Bars

One of the earliest impact problems we attempted to solve was that for an elastic bar impacting a rigid wall. Our initiatory results for this problem were qualitatively correct but not very accurate, (see [1] Fig. 12). Improvements in our understanding of the numerical algorithm as well as our continued sharpening of the impact and release conditions programmed in FEAP has enabled us to dramatically improve the accuracy obtainable in impact problems. We shall illustrate this by the example of two bars impacting and then releasing, Fig. I-12. The tremendous improvement in accuracy can be seen by compairing the present results, Figs. I-13 to I-15, with those

TABLE I-1

COMPARISON OF NUMERICAL RESULTS FOR SPHERE IMPACT PROBLEM WITH QUASISTATIC HERTZ SOLUTION

V = -3.	a	t	p
Hertz	1.00	.197	294.
Mesh 4	1.00	.18	330.
Mesh 5	1.00	.19	352.

V = -.8	a	t	p
Hertz	.59	.256	60.2
Mesh 4	.6	.24	65.

a = maximum contact radius

t = duration of contact

p = maximum contact force

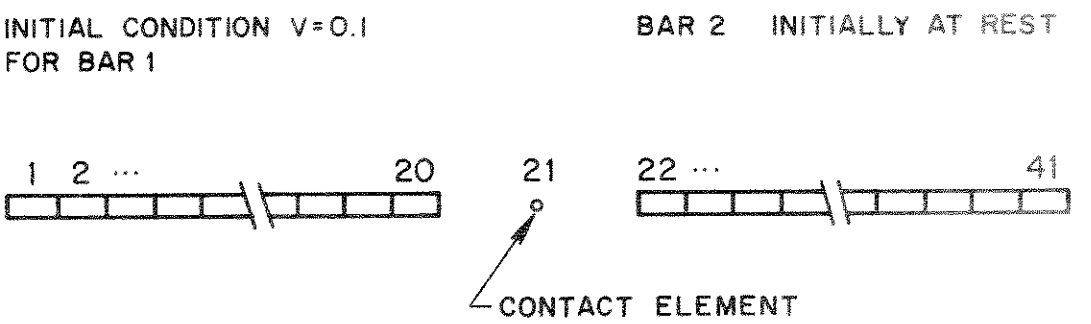

DATA:

$L = 10$	(LENGTH / BAR)
$E = 100$	(YOUNG'S MODULUS)
$\rho = 0.01$	(DENSITY)
$A = 1$	(AREA)
$\Delta t = 0.005$	(TIME STEP)

FIGURE I-12

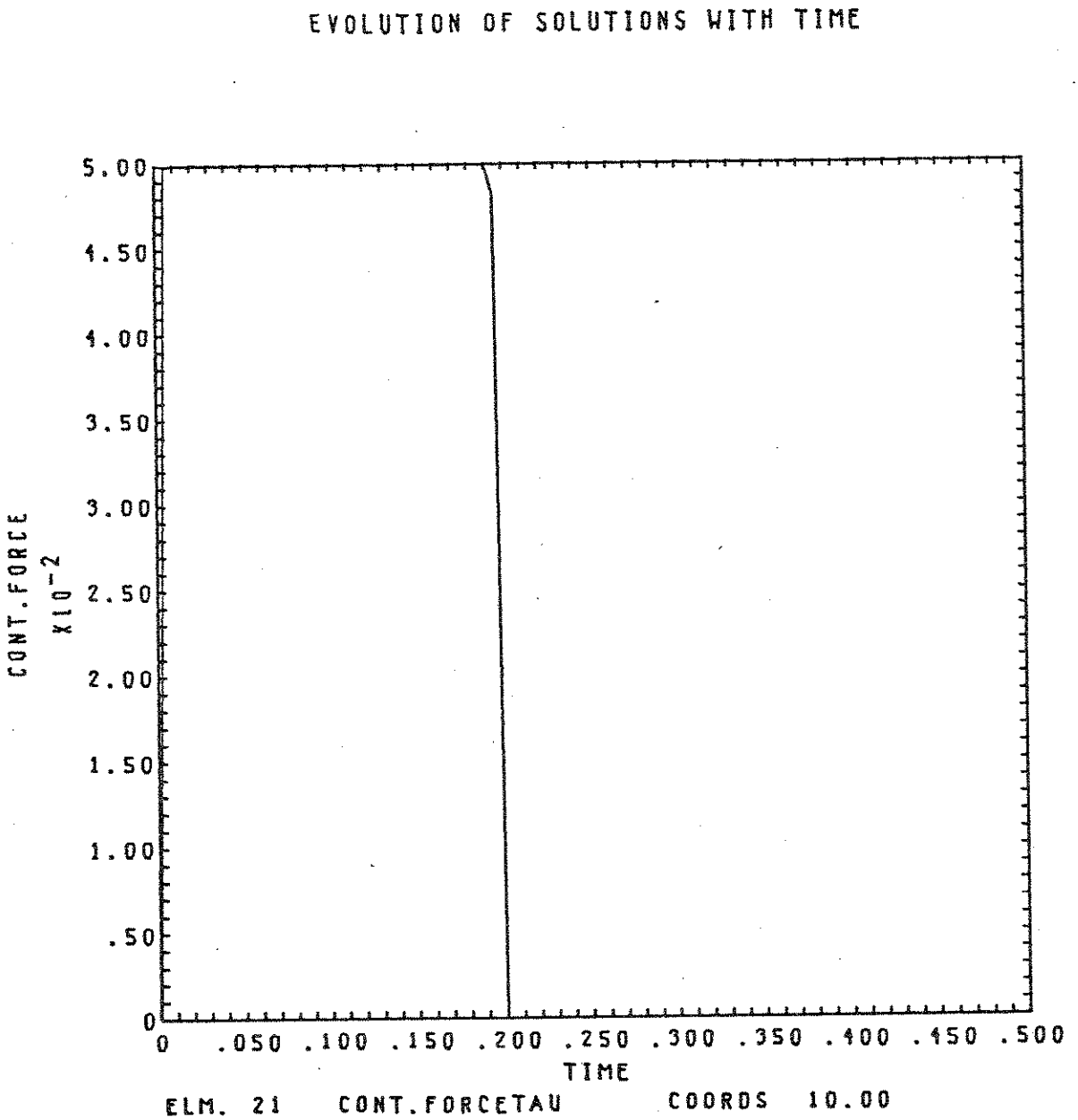
EVOLUTION OF SOLUTIONS WITH TIME
CONT.FORCE
X10-2
5.00
4.50
4.00
3.50
3.00
2.50
2.00
1.50
1.00
.50
0
0 .050 .100 .150 .200 .250 .300 .350 .400 .450 .500
TIME
ELM. 21 CONT.FORCETAU COORDS 10.00

Figure I-13

EVOLUTION OF SOLUTIONS WITH TIME

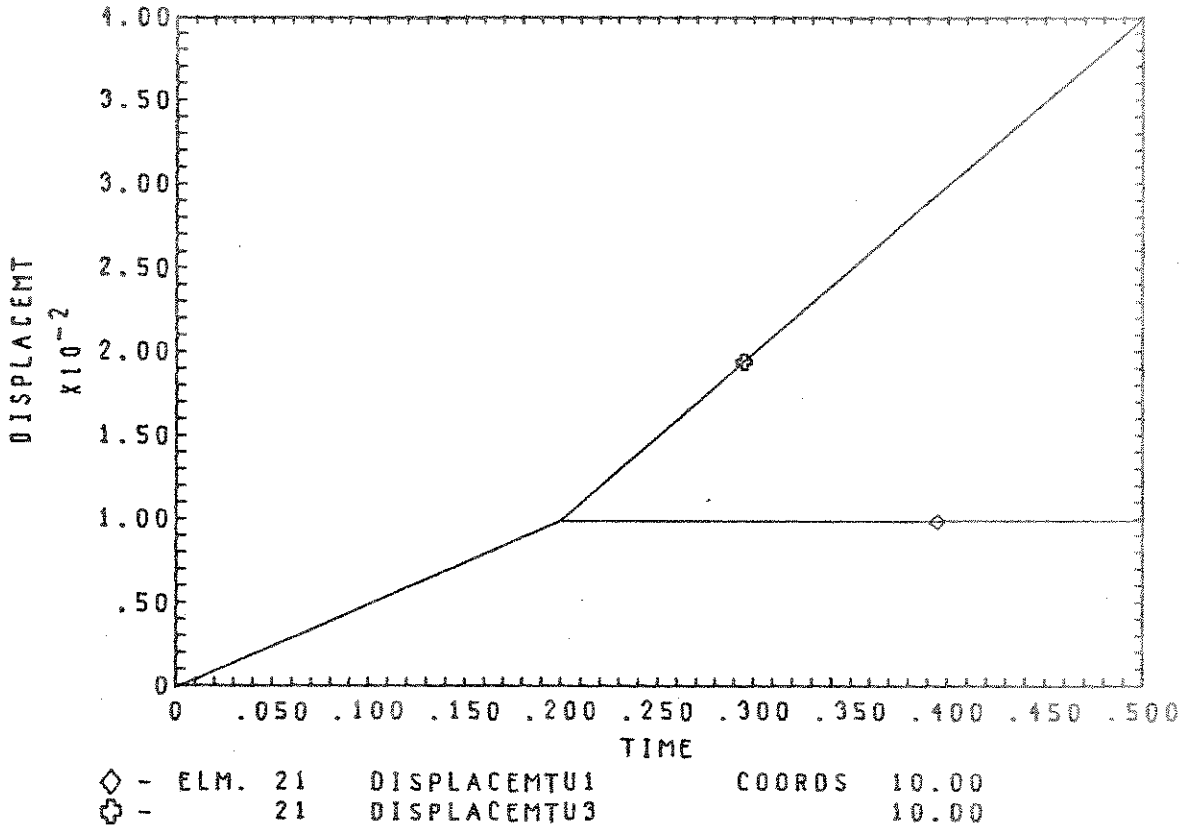

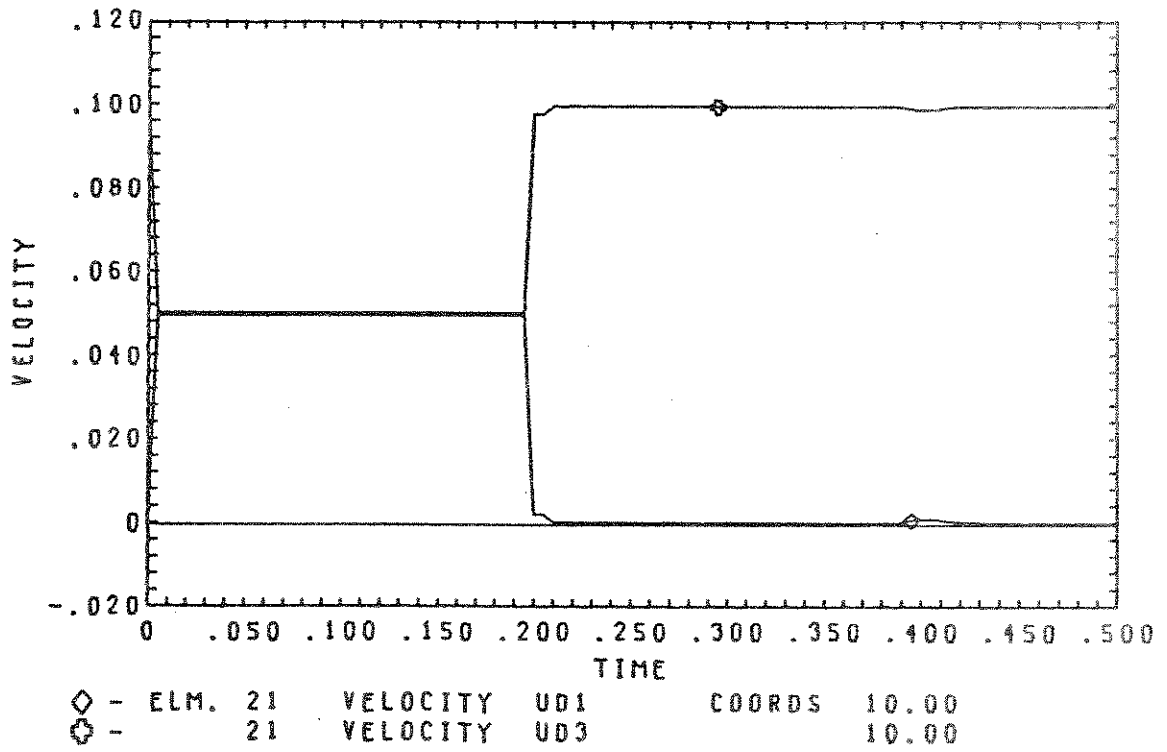

Figure I-14

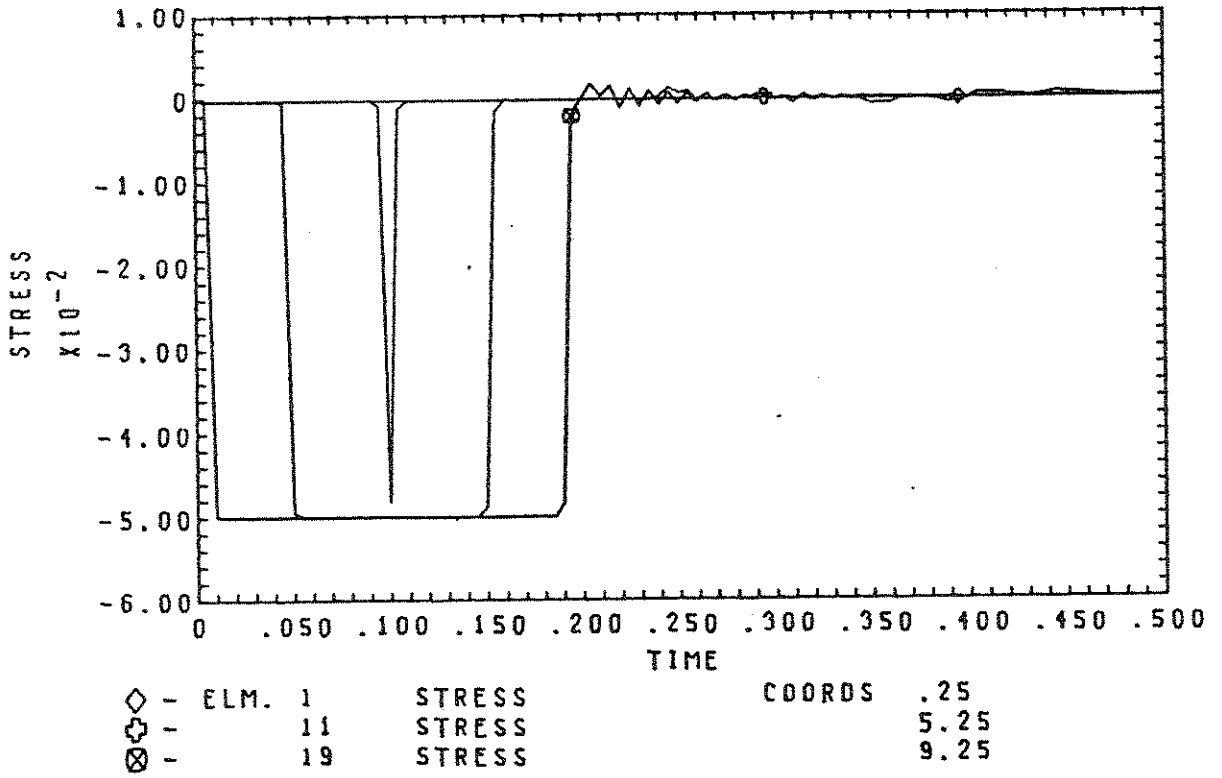
1.00
0
-1.00
-2.00
-3.00
-4.00
-5.00
-6.00
STRESS
X10-2
0 .050 .100 .150 .200 .250 .300 .350 .400 .450 .500
TIME
◇ - ELM. 1 STRESS COORDS .25
- 11 STRESS 5.25
⊗ - 19 STRESS 9.25

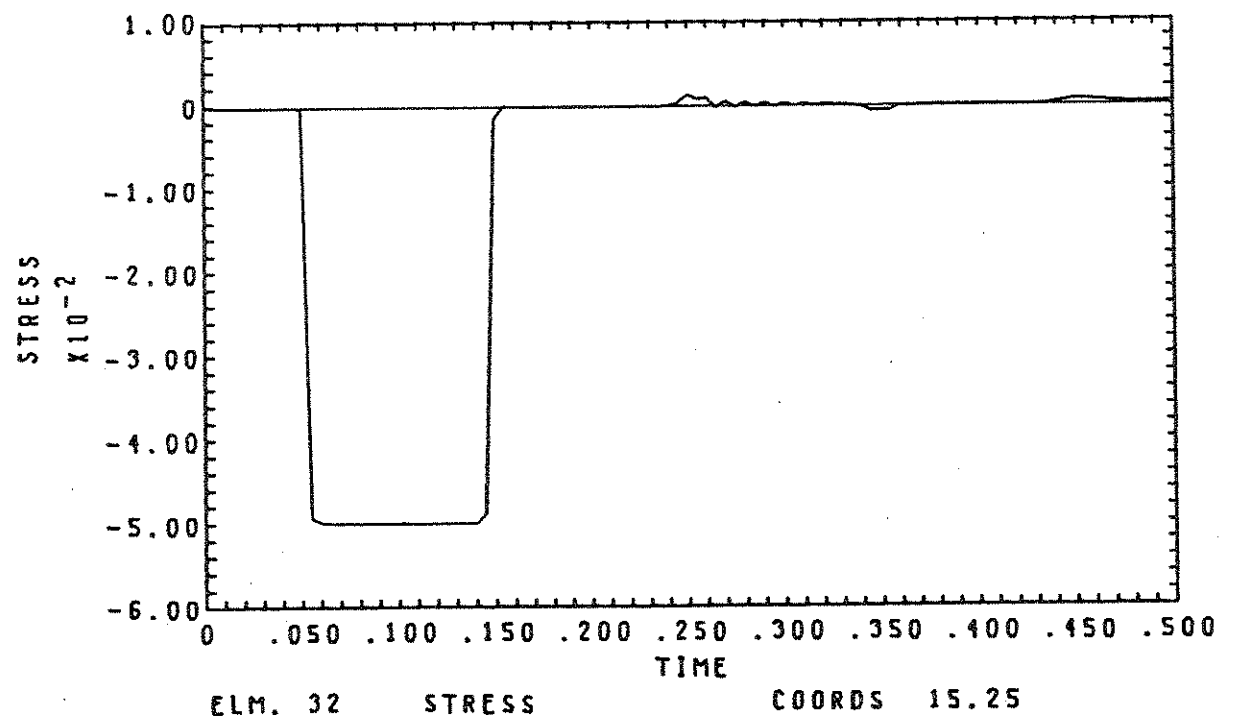
1.00
0
-1.00
-2.00
-3.00
-4.00
-5.00
-6.00
STRESS
X10-2
0 .050 .100 .150 .200 .250 .300 .350 .400 .450 .500
TIME
ELM. 32 STRESS COORDS 15.25

Figure I-15

for one bar impacting a rigid wall (a simpler problem!) contained in [1]. We have not bothered to plot the exact solution in comparison with our results since the differences are so small. Note how effectively the impact conditions ([1], §7) bring the contact force from zero to the exact value in one time step without any overshoot (Fig. I-13). The release (at t=.2) is also very crisp. This is due to the release conditions which work analogously to the impact conditions. The slight perturbation from the exact solution, which is due to the Newmark algorithm, could be made to go away completely with mesh refinement. This problem, although trivial analytically, clearly demonstrates the necessity of imposing impact conditions (as discussed in [1], Sections 7 and 12) when contact is being made. In fact, our initial numerical experiments for the one bar impacting a rigid wall problem, run without impact conditions, yielded results which were completely inaccurate.

We have also found, in the course of our work, that one must impose release conditions, analogous to the impact conditions, to accomplish a clean separation free of spurious "release waves". This fact is illustrated in Figs. I-16 to I-18 which are the results of a problem in which we have looped around the release conditions programmed in FEAP. Spurious spikes are visible in the latter part of the solution which is a direct result of not imposing the release conditions (cf. Figs. I-13 - 15).

As we have remarked before, this problem is quite simple to solve analytically, but nevertheless is a source of considerable insight as regards impact-release phenomena. Since the definition of the contact surface (a point) is trivial we are able to focus in

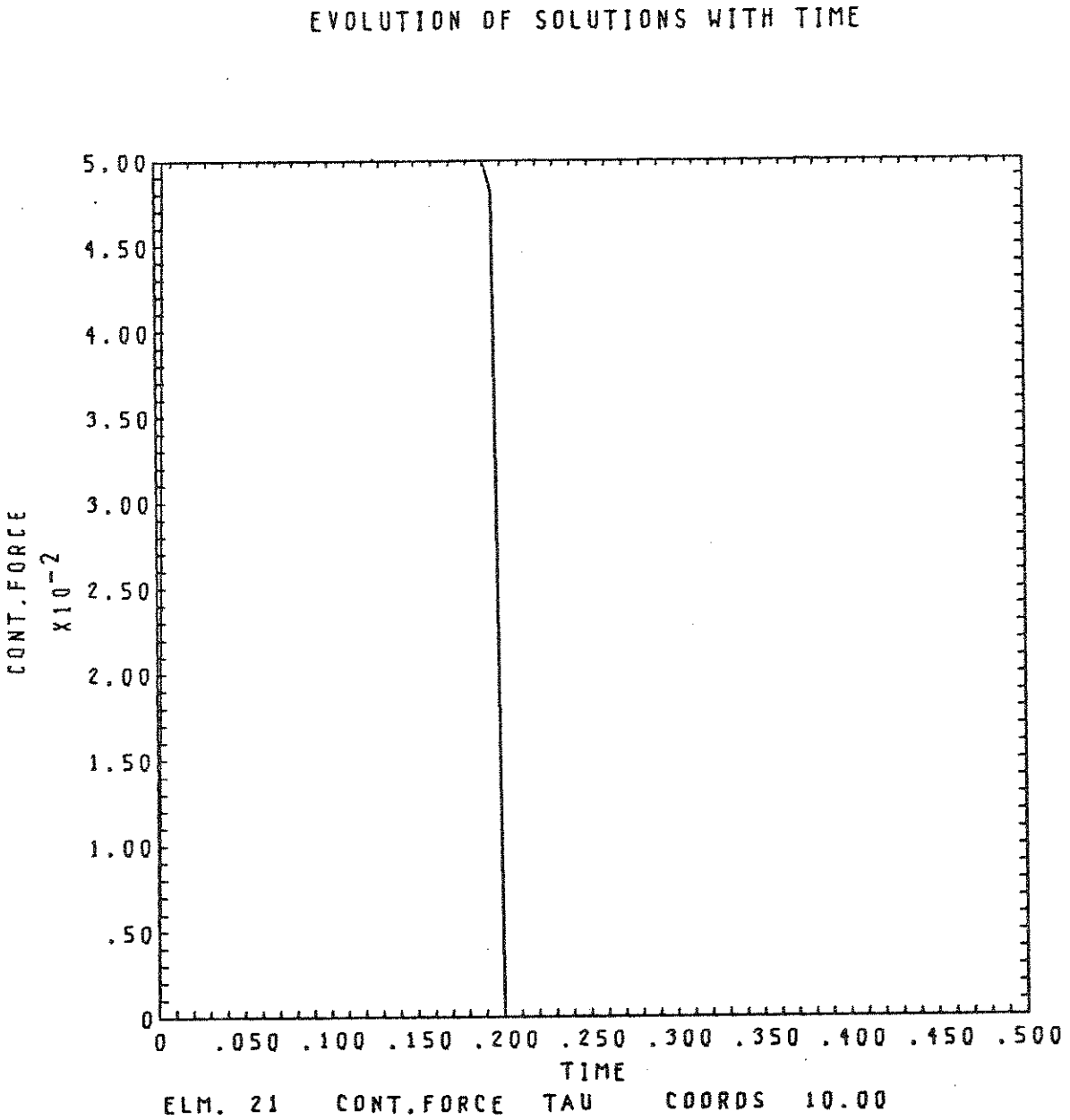
EVOLUTION OF SOLUTIONS WITH TIME
CONT.FORCE
X10⁻²
5.00
4.50
4.00
3.50
3.00
2.50
2.00
1.50
1.00
.50
0
0 .050 .100 .150 .200 .250 .300 .350 .400 .450 .500
TIME
ELM. 21 CONT.FORCE TAU COORDS 10.00

Figure I-16

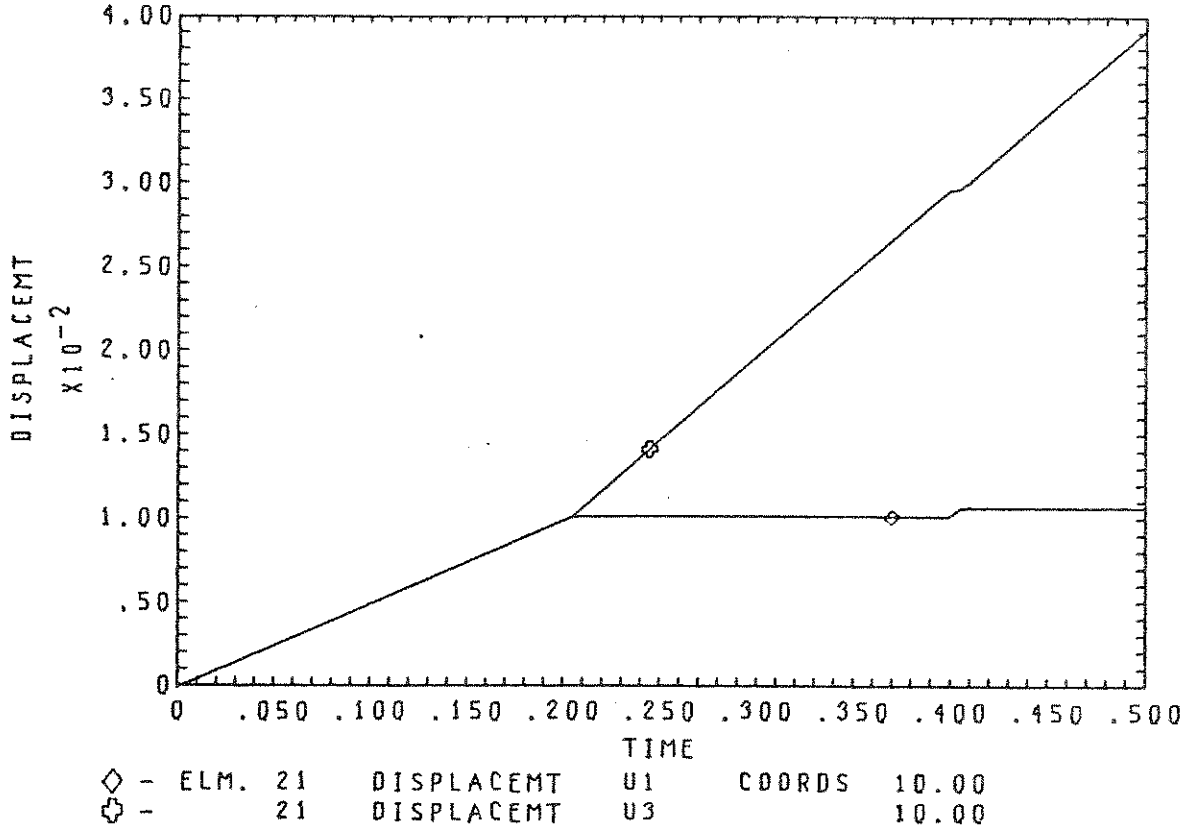
DISPLACEMT
X10^{-2}
4.00
3.50
3.00
2.50
2.00
1.50
1.00
.50
0
0 .050 .100 .150 .200 .250 .300 .350 .400 .450 .500
TIME
◇ - ELM. 21 DISPLACEMT U1 COORDS 10.00
◇ - 21 DISPLACEMT U3 10.00

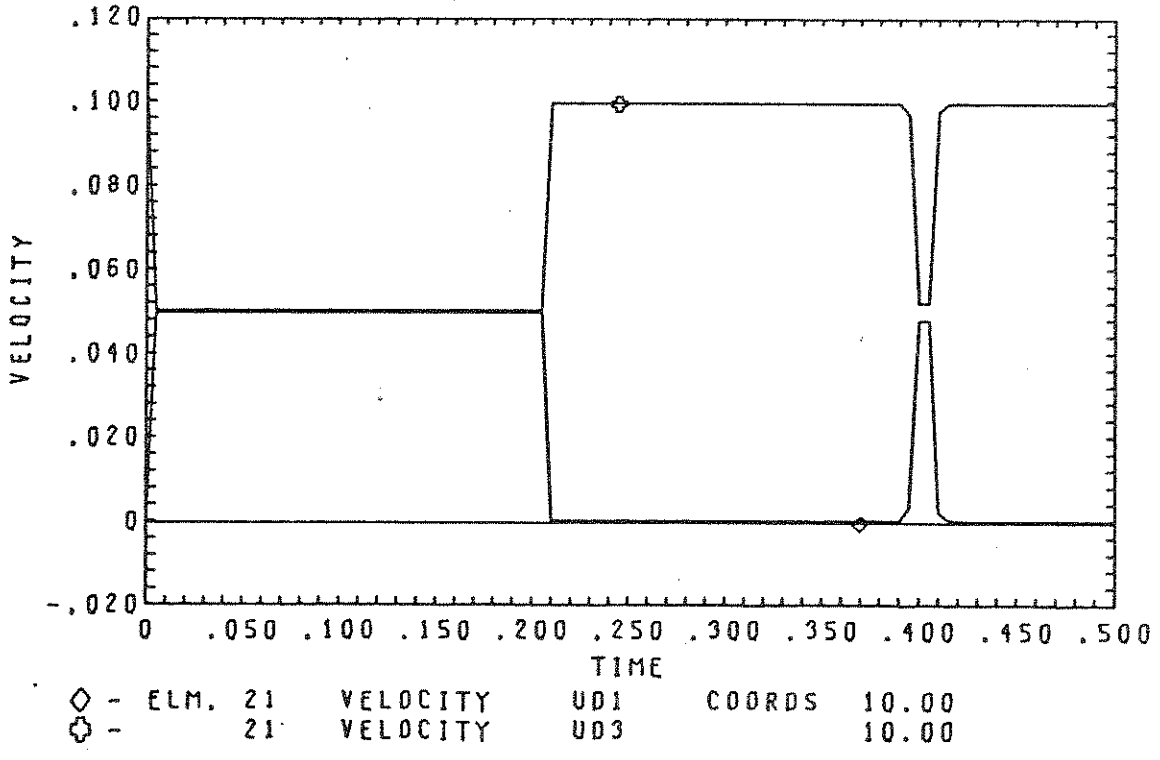
VELOCITY
.120
.100
.080
.060
.040
.020
0
-.020
0 .050 .100 .150 .200 .250 .300 .350 .400 .450 .500
TIME
◇ - ELM. 21 VELOCITY UD1 COORDS 10.00
◇ - 21 VELOCITY UD3 10.00

Figure I-17

EVOLUTION OF SOLUTIONS WITH TIME

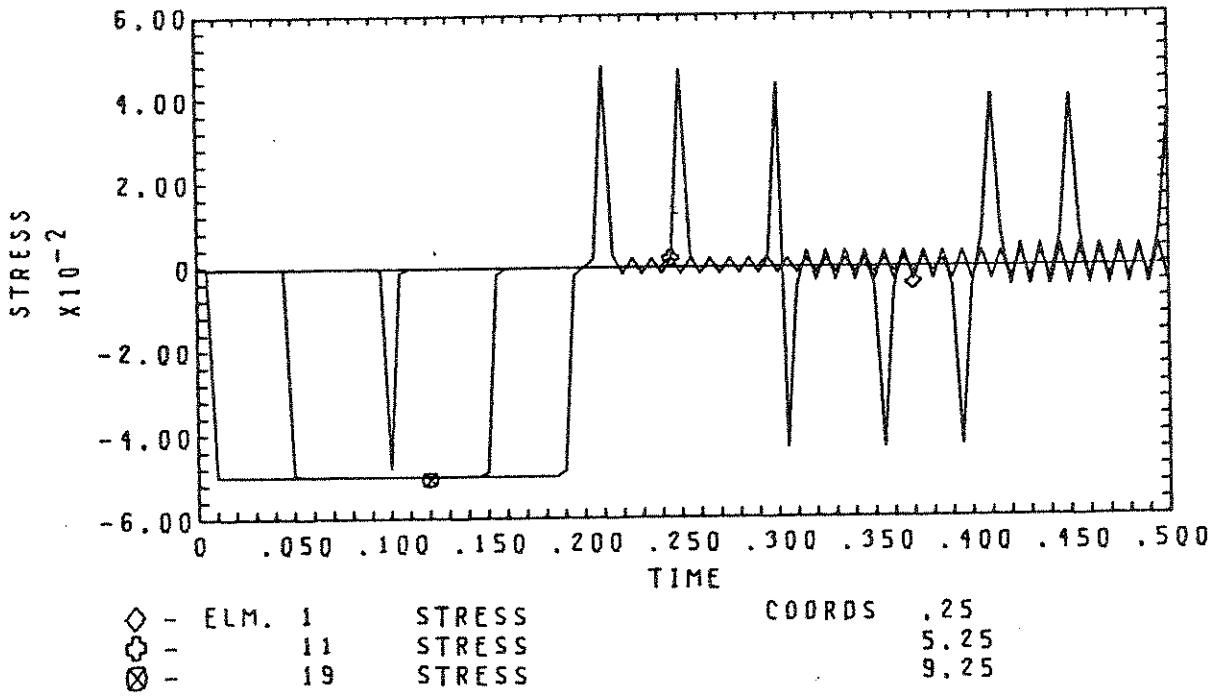

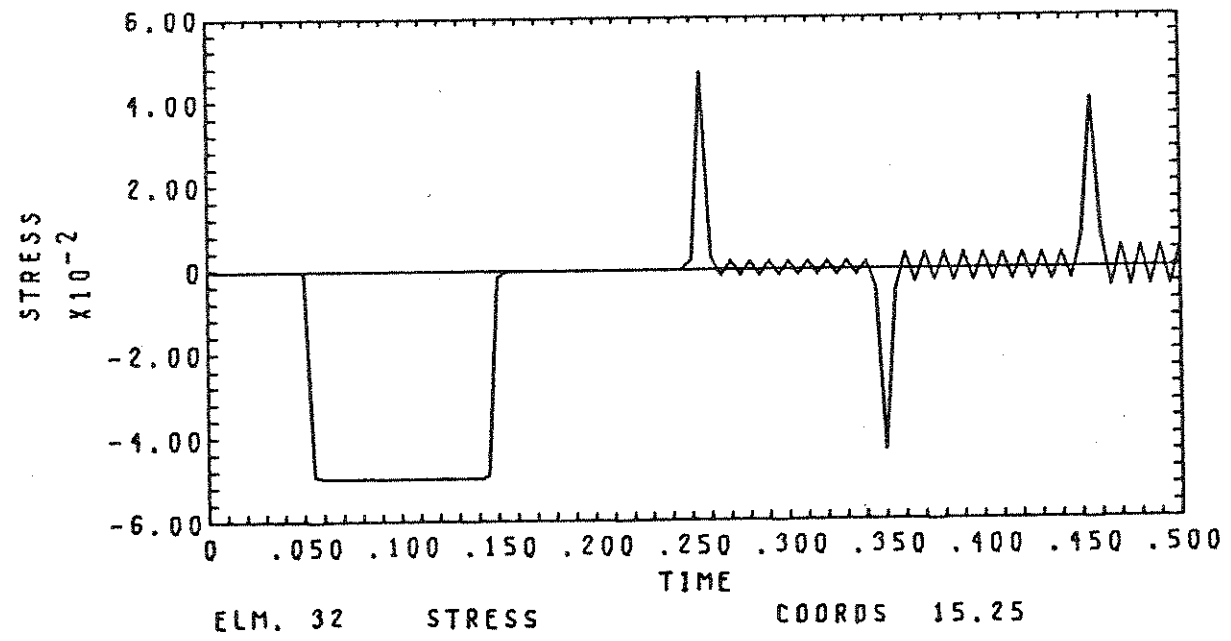

Figure I-18

completely on the importance of achieving a theoretically correct impact and release. We have felt for some time (cf. our arguments in Section 7 of [1]) that being able to accurately solve the wave propapation problem for impacting bars was a key step towards solving highly detailed wave propagation problems in general three-dimensional bodies. Our results, which demonstrate the veracity and necessity of the imposed impact/release conditions as well as the potential accuracy of the overall algorithm, indicate that we are well on the way to developing the capabilities for solving physical problems of interest.

A nonlinear problem of this size (i.e., 41 degrees of freedom, 100 time steps, postprocessing for 9 plots, etc.) is currently costing us in the neighborhood of $9.00 on the University of California's CDC 6400 and utilizes about 60 CPU seconds.

II. Numerical Scheme for the Kinematically Nonlinear Contact/Impact Problem

1. Introduction

In this aspect of our work we have endeavored to design a scheme which is a logical generalization of the one developed for the class of Hertzian problems. That is, we have set for ourselves the design requirement that the full kinematically nonlinear scheme reduce to the Hertzian formulation under the appropriate circumstances. We view this as a reasonable approach since the Hertzian scheme is working out extremely well computationally and, based upon what we have learned in the course of its implementation, we believe many of its features can be instilled into a nonlinear formulation. Before describing our proposed nonlinear scheme we will briefly describe the Hertzian formulation so as to exhibit how the nonlinear scheme satisfies the aforementioned design requirement.

2. Hertzian Scheme

For background regarding this section the reader is referred to our initiatory work [1].

Recall that we term Hertzian problems ones for which the contact surface is approximately planar and the bodies have undergone small straining in the neighborhood of the contact surface. Specifically, we make the following assumptions:

(i) The unit normal vector with respect to the contact surface c is $\underset{\sim}{n} \overset{\text{def}}{=} n_i \underset{\sim}{e}_i \approx \underset{\sim}{e}_3$, where the n_i indicate components with respect to the standard basis $\{e_i\}_1^3$ for $\mathbb{R}^3$, (see Fig. II-1).

(ii) The ratio of area elements on the contact surface between the deformed and undeformed bodies differs negligibly from unity.

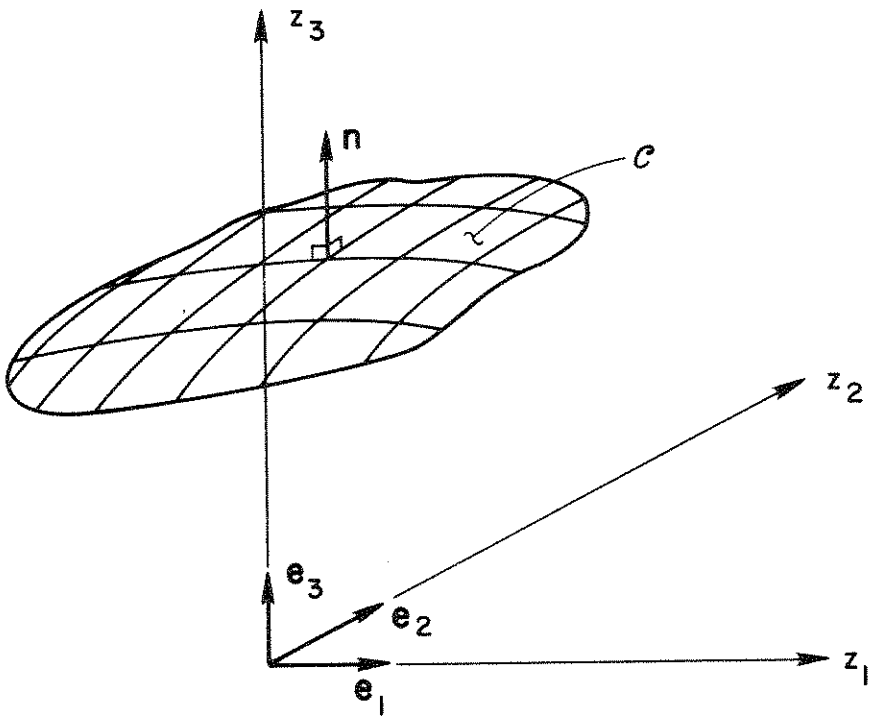

FIGURE II-1

Thus the Cauchy and Piola-Kirchhoff traction vectors for body number α ($\underset{\sim}{t}^{\alpha}$ and $\underset{\sim}{T}^{\alpha}$, respectively) are approximately equal, i.e., $\underset{\sim}{t}^{\alpha} \approx \underset{\sim}{T}^{\alpha}$.

Assumptions (i) and (ii) together imply that

$$t_3^{\alpha} \approx \underset{\sim}{t}^{\alpha} \cdot \underset{\sim}{n} \approx \underset{\sim}{T}^{\alpha} \cdot \underset{\sim}{n} \approx T_3^{\alpha} ,$$

$$(t_1^{\alpha}, t_2^{\alpha}, 0) \approx \underset{\sim}{t}^{\alpha} - (\underset{\sim}{t}^{\alpha} \cdot \underset{\sim}{n})\underset{\sim}{n} \approx \underset{\sim}{T}^{\alpha} - (\underset{\sim}{T}^{\alpha} \cdot \underset{\sim}{n})\ \underset{\sim}{n} \approx (T_1^{\alpha}, T_2^{\alpha}, 0) .$$

(iii) Material points which eventually contact have, to the first order, the same initial coordinates z_1, z_2. This is depicted in Fig. II-2.

We emphasize that the realm of applicability of our formulation involving the above assumptions is considerably greater than that to which Hertz' classical theory applies.

The methods we use to discretize problems into finite element models are standard (see, e.g., [2]) except for our simulation of the contact surface which we shall now describe.

Let us assume for the moment that two bodies are in contact along the surface c. If we add to a standard variational formulation for two independent bodies, (see, e.g., [1]) a term of the form

$$\int_c \underset{\sim}{\tau} \cdot (\underset{\sim}{x}^1 - \underset{\sim}{x}^2)\, dc, \qquad \text{(II-1)}$$

where $\underset{\sim}{x}^{\alpha}$ are the deformed coordinates of material points in body number α, the enforcement of compatibility along the surface c will be achieved by way of taking independent variations of $\underset{\sim}{\tau}$. $\underset{\sim}{\tau}$ is interpreted as the traction vector across the contact surface. We note that, by assumption (i) above, c may be replaced in (II-1) by c, its projection upon the z_1, z_2 - plane.

Our finite element discretization of (II-1) is achieved by availing ourselves of the particularly simple nature of (II-1), i.e.,

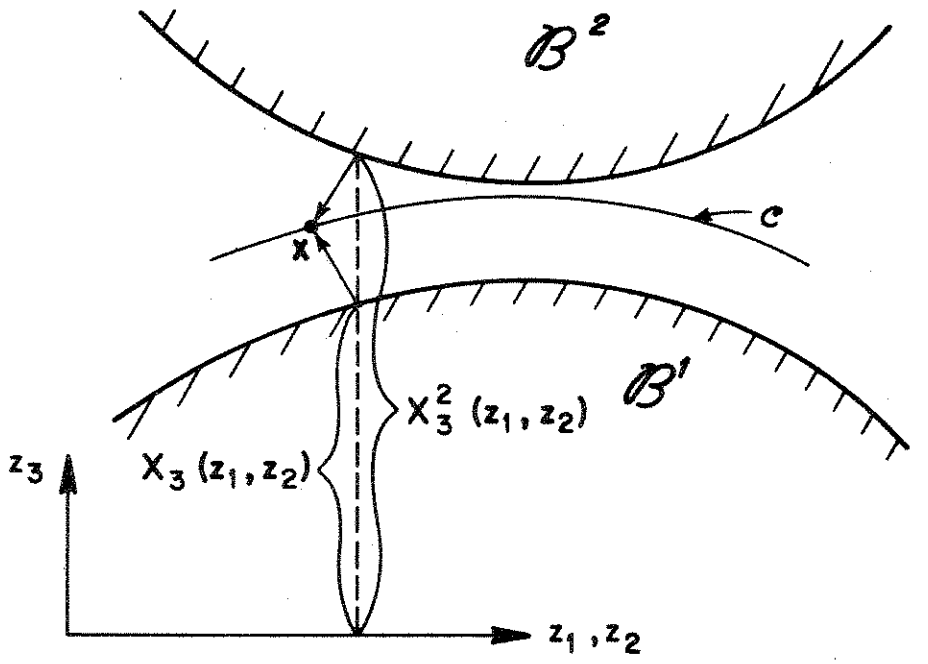

FIGURE II-2

there are no derivatives of $\underset{\sim}{\tau}$ or $\underset{\sim}{x}^{\alpha}$. Thus we may assume that $\underset{\sim}{\tau}$ consists of Dirac delta functions located at nodal points, as long as the finite element displacement functions are continuous at the nodes, which is assured. Thus (II-1) becomes in this case

$$\sum_{i=1}^{3} \sum_{j=1}^{N} \tau_{ij} \left(x_{ij}^{1} - x_{ij}^{2}\right) , \tag{II-2}$$

where i = 1, 2, 3 refers to the spatial direction of components and N is the total number of pairs of nodes designated as candidates for contact (see Fig. II-3). The τ_{ij} are interpreted as nodal contact forces.

(II-1) and (II-2) apply when there are tangential as well as normal contact forces. To achieve a frictionless condition on the contact surface we simply delete the i = 1, 2 terms in (II-1) and (II-2); namely

$$\begin{aligned} &\int_{C} \tau \left(x^{1} - x^{2}\right) , \\ &\sum_{j=1}^{N} \tau_{j} \left(x_{j}^{1} - x_{j}^{2}\right), \end{aligned} \tag{II-3}$$

where for simplicity we have omitted the subscript 3 on τ and x^{α}. Here τ_{j} is interpreted as the nodal contact force in the normal direction. To simplify our presentation we will henceforth only discuss the frictionless case (II-3).

In assembling our global matrix equations we include the τ_{j}'s in our vector of unknowns along with the nodal displacement components. Thus we like to think of (II-3) as giving rise to a contact element stiffness matrix, which for the j^{th} contact point is

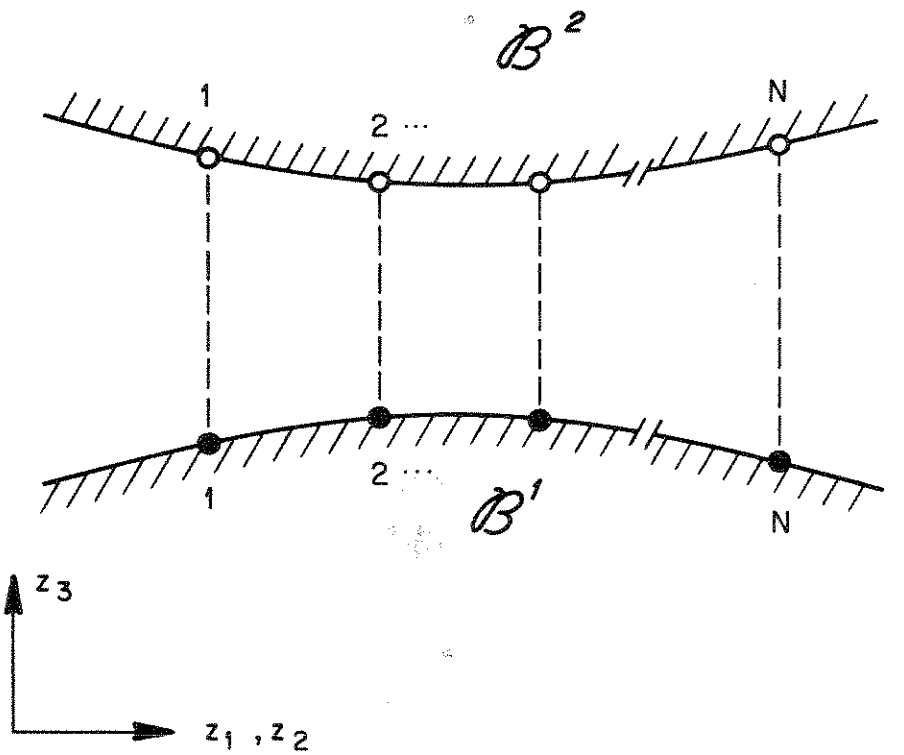

FIGURE II-3 SCHEMATIC OF INITIAL CONFIGURATION OF BODIES AND ALIGNMENT OF CANDIDATE CONTACT NODES FOR THE HERTZIAN CASE.

$$\begin{bmatrix} 0 & 1 & 0 \\ 1 & 0 & -1 \\ 0 & -1 & 0 \end{bmatrix} \begin{Bmatrix} x_j^1 \\ \tau_j \\ x_j^2 \end{Bmatrix} \tag{II-4}$$

When the nodes corresponding to the j^{th} contact point are in contact we add (II-4) to the global stiffness matrix. Otherwise we replace (II-4) by

$$\begin{bmatrix} 0 & 0 & 0 \\ 0 & 1 & 0 \\ 0 & 0 & 0 \end{bmatrix} \begin{Bmatrix} x_j^1 \\ \tau_j \\ x_j^2 \end{Bmatrix} \tag{II-5}$$

which uncouples the two nodes corresponding to the j^{th} contact point and results in $\tau_j = 0$.

The preceding description gives a rough idea of how the basic structure of the matrix equations is changed to account for Hertzian contact.

The static aspects of the Hertzian algorithm (above) are relatively simple. However, the dynamic aspects, especially the impact/release conditions, are quite delicate. Since these appear in an incomplete form in [1] we summarize this aspect of our work here.

For simplicity, we shall consider the frictionless case and isolate one pair of candidate contact nodes. The equations of motion for these nodes will be denoted

$$\begin{aligned} M^1 \ddot{u}^1 + K^1(\underset{\sim}{u}^1) + \tau &= 0, \\ M^2 \ddot{u}^2 + K^2(\underset{\sim}{u}^2) - \tau &= 0, \end{aligned} \tag{II-6}$$

where the superscripts indicate the body number, M^α is the lumped mass coefficient, $K^\alpha(\underset{\sim}{u}^\alpha)$ is the elastic force and τ is the contact force. If the bodies are not in contact $\tau = 0$; otherwise $\tau > 0$.

Let us suppose that at the end of the previous time step these candidate nodes were not in contact. Furthermore, let us assume that in the process of computing the present state contact has been made. This occurs during an iteration whenever

$$\text{(i)} \quad d \overset{\text{def.}}{=} x^1 - x^2 < -TOL$$

or (II-7)

$$\text{(ii)} \quad d < TOL \text{ and } \tau > 0$$

where TOL^* is a small positive number which acts as a safeguard against round-off. This logic is displayed graphically in Fig. II-4. As a result of coming into contact, the algorithm makes the displacements compatible, i.e., $u^2 - u^1 = d_o \overset{\text{def.}}{=} X^1 - X^2$, where X^1, X^2 are the coordinates of the particles in the initial configuration. However, the velocities $\dot{u}^1$, $\dot{u}^2$ and accelerations $\ddot{u}^1$, $\ddot{u}^2$ are left as computed by the algorithm. It is at this point that we impose the impact conditions (see the discussion in Sections 7 and 12 of [1]). We denote by V_+, τ_+ and $\ddot{u}_+$ the corrected values of velocity, contact force and acceleration assigned to the pair of nodes in contact. They are given as follows:

$$V_+ = \frac{\left(\rho_o{}^2 U^2 \dot{u}^2_{-1} - \rho_o{}^1 U^1 \dot{u}^1_{-1}\right)}{\left(\rho_o{}^2 U^2 - \rho_o{}^1 U^1\right)}$$

$$\tau_+ = \tau_- - \frac{M^1 M^2}{(M^1 + M^2)} (\ddot{u}^2_- - \ddot{u}^1_-) , \qquad \text{(II-8)}$$

$$\ddot{u}_+ = \frac{(M^1 \ddot{u}^1_- + M^2 \ddot{u}^2_-)}{(M^1 + M^2)} ,$$

*Currently we are using $TOL = 10^{-10}$ in FEAP.

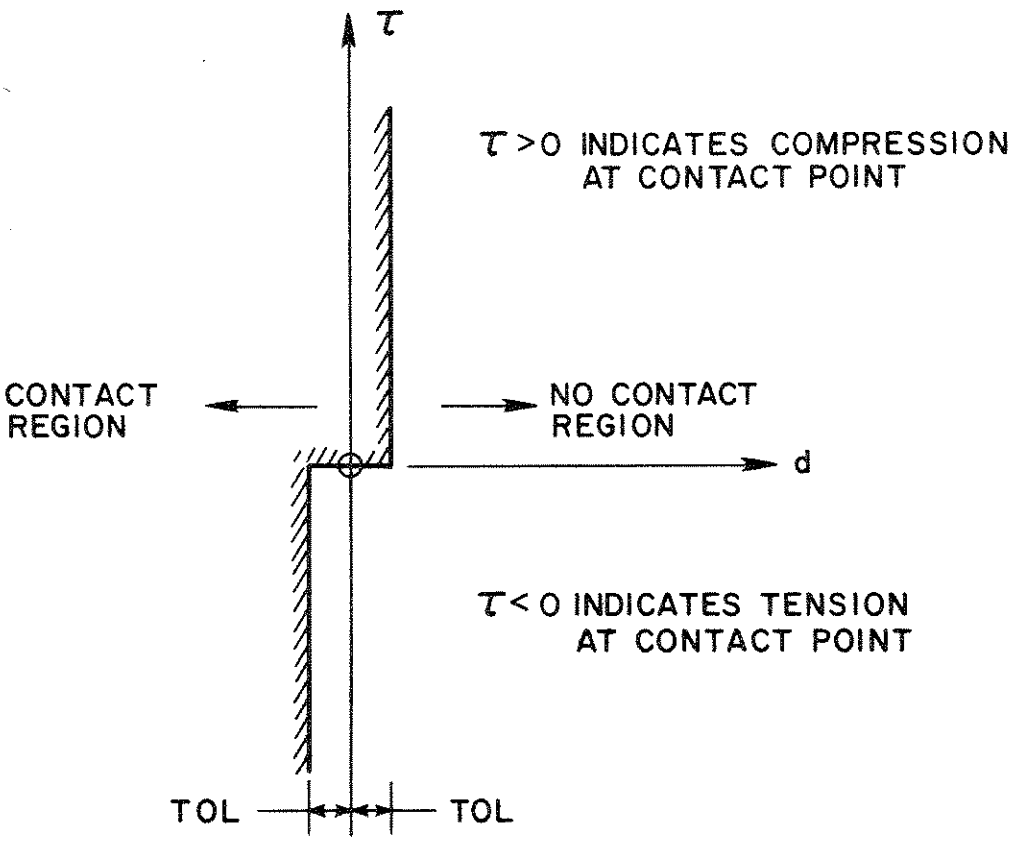
τ
τ >0 INDICATES COMPRESSION
AT CONTACT POINT
CONTACT
REGION
NO CONTACT
REGION
d
τ< 0 INDICATES TENSION
AT CONTACT POINT
TOL
TOL

FIGURE II-4

where ρ_0^{α} is the density of body α in the initial configuration, U^{α} is the material velocity of a shock wave in body α (see Section 7 of [1] for further details), the subscript (-1) refers to values taken at the end of the previous time step and the subscript (-) indicates values taken at the end of the last iteration of the present time step. Note that the right-hand side of $(II\text{-}8)_1$, depends on data computed prior to impact (i.e., $\dot{u}^1_{-1}$, $\dot{u}^2_{-1}$). This is consistent with the theory developed in Section 7 of [1] and is important in numerical computations. For example, using data from the last iteration of the present time step (i.e., $\dot{u}^1_-$, $\dot{u}^2_-$) leads to markedly inferior numerical results (e.g., spike overheats and oscillations about the correct values). On the other hand τ_+ and $\ddot{u}_+$ are computed from data obtained in the last iteration (i.e., τ_-, $\ddot{u}^1_-$, $\ddot{u}^2_-$). The argument for this goes as follows: The impact theory tells us that in the post-impact state there is a unique value of τ_+ and $\ddot{u}_+$ assigned to the contact point. Since the values of u^1_- and u^2_- are already compatible we employ (II-6) to solve for τ_+ and $\ddot{u}_+$. That is we set

$$\begin{aligned} M^1 \ddot{u}_+ + K^1(\underset{\sim}{u}^1_-) + \tau_+ &= 0 \quad , \\ M^2 \ddot{u}_+ + K^2(\underset{\sim}{u}^2_-) - \tau_+ &= 0 \quad , \end{aligned} \tag{II-9}$$

and subtract (II-9) from (II-6) evaluated at the previous iteration:

$$\begin{aligned} M^1 \ddot{u}^1_- + K^1(\underset{\sim}{u}^1_-) + \tau_- &= 0 \quad , \\ M^2 \ddot{u}^2_- + K^2(\underset{\sim}{u}^2_-) - \tau_- &= 0 \quad . \end{aligned} \tag{II-10}$$

This is how we arrive at $(II\text{-}8)_{2,3}$. Satisfaction of the equations of motion is automatically achieved for the post-impact state as a result of (II-9).

Now we shall describe the release conditions. These stem from the same concepts as the impact conditions. Prior to studying them

and including them in FEAP we surmised that they might be necessary. Vivid numerical evidence was obtained in confirmation of this (cf. Section I-3 of this report).

One way to look at the release conditions is to view them as impact conditions with time running backwards. Thus we simply invert $(53)_{1,2}$ of [1] to obtain the post-release velocities V_+^1 and V_+^2 from the pre-release data τ_{-1} and V_{-1}:

$$\begin{aligned} V_+^1 &= V_{-1} - \tau_{-1}/\rho_o{}^1U^1A^1 \ , \\ V_+^2 &= V_{-1} + \tau_{-1}/\rho_o{}^2U^2A^2 \ , \end{aligned} \tag{II-11}$$

where A^1, A^2 are area weighting factors for the respective candidate nodes. Simultaneously we need τ_+ to be equal to zero. We set $\tau_+ = 0$ and adjust the accelerations in (II-6) so that this change maintains satisfaction of the equations of motion. The computation is analogous to the one in which we calculated $(II\text{-}8)_{2,3}$:

$$\begin{aligned} \ddot{u}_+^1 &= \ddot{u}_-^1 + \tau_-/M^1 \ , \\ \ddot{u}_+^2 &= \ddot{u}_-^2 - \tau_-/M^2 \ ; \end{aligned} \tag{II-12}$$

where here $\ddot{u}_+^1$ and $\ddot{u}_+^2$ are the corrected post-release accelerations and $\ddot{u}_-^1$, $\ddot{u}_-^2$ and τ_- are the values computed from the last iteration of the present time step.

We determine whether or not release has occurred in the following way: If $\tau < 0$ (tension across the contact surface in any iteration) we release; if $\tau_- > 0$, but less than 2% of the previous time step value (τ_{-1}), we also release. Otherwise we retain contact. The last release case above was arrived at from numerical experimentation. For example, problems were run for releasing bars in which the

theoretical drop-off of τ was 100% in one time-step (shock waves). Our numerical computations predicted this drop-off quite accurately producing a positive τ of less than 10^{-3} times the previous value. Interpreting this as contact, the algorithm did not release the bars until the next time step at which time the update indicated in (II-11) and (II-12) had negligible effect due to the very small value of τ_-. We deduced from cases like this the criterion above.

The only pitfall of using this criterion can be seen as follows: Suppose the actual drop-off during a time step in a problem is greater than 98% of the previous value, but the exact solution from this point on is constant at some small positive τ. The algorithm would release and not join the nodes until the next time step. From here on everything would run as it should.

With this as background we are in a position to describe the essential ideas behind our proposed kinematically nonlinear contact scheme.

3. Kinematically Nonlinear Scheme

The starting point for the nonlinear scheme is again with Equation (II-1). We note that there are no assumptions involved in the statement of (II-1) and that it applies to the fully nonlinear case. However, the condition that σ and its projection c may be identified in (II-1) is no longer applicable, for in the kinematically nonlinear case σ will in general not be planar.

To explicate as quickly as possible the nature of our proposed scheme we shall deal with a simple case. Namely we shall assume the problem to be two-dimensional (e.g., the axisymmetric contact-impact of three-dimensional bodies) and we shall assume that the element

displacement functions are linear between nodes. The ideas which we are about to present are by no means restricted to these assumptions. However, these assumptions will allow a concise and clear exposition of the main concepts being employed.

Our first step is to associate to each body a set of candidate contact nodes. Of course these nodes will not, in general, meet to the first-order as they do in the class of Hertzian problems. In the present case no restriction will be made as to the number of candidate nodes, i.e., the number for body 1, say, N^1, will not be equal, in general, to that for body 2, say, N^2. Without loss of generality we shall assume $N^1 \leq N^2$ (see Fig. II-5). To each of the candidate nodes of body 1, we shall assign a contact force vector $\underset{\sim}{\tau}_j$, $j = 1, \ldots N^1$. This may be interpreted in the same way as the Hertzian case, i.e., the $\underset{\sim}{\tau}$ vector field is assumed to consist of Dirac delta functions located at the nodal points.

When contact does occur in the nonlinear case it will not be "at the nodes" as in the Hertzian case. Thus (II-2) has no meaning in the present situation. Rather in its place one derives

$$\sum_{i=1}^{2} \sum_{j=1}^{N^1} \sum_{k=1}^{N^2} \tau_{ij}(x_{ij}^{1} - a_{jk}\, x_{ik}^{2}) \qquad \text{(II-13)}$$

where the $N^1 \times N^2$ matrix $\underset{\sim}{A} = [a_{jk}]$ represents the integration of the Dirac delta functions times the displacement interpolation functions of body 2 over the contact surface c. Rather than actually perform these integrations, one can construct $\underset{\sim}{A}$ directly from the physical situation.

In constructing the global equations we again include the τ_{ij}'s among the nodal unknowns. To see the difference between the present

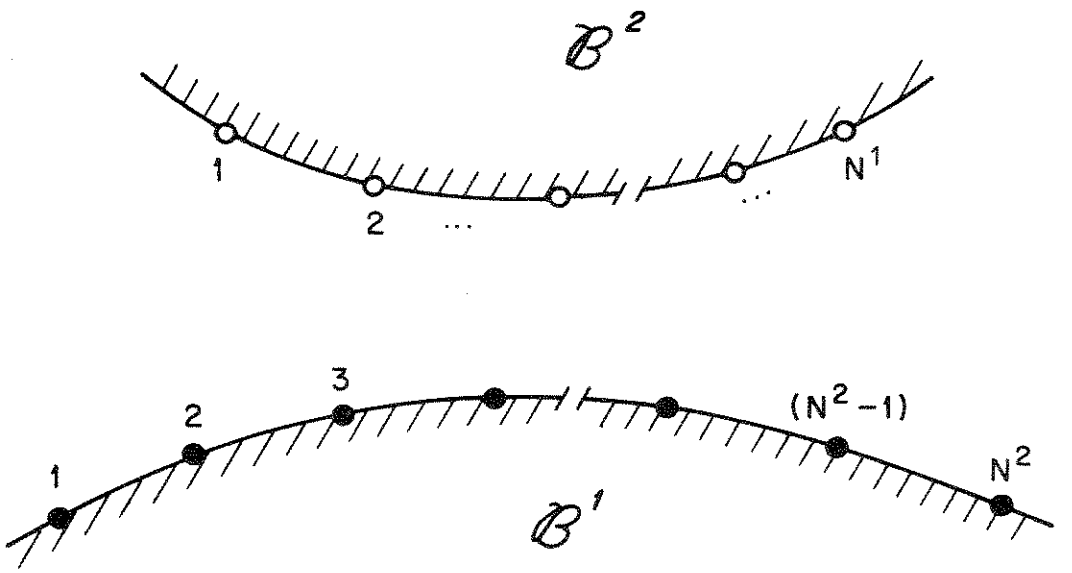

FIGURE II-5 CANDIDATE CONTACT NODES OF BODIES IN THEIR INITIAL CONFIGURATION FOR THE NONLINEAR CASE.

setup and the previous (see, e.g., (II-5)) we shall consider a simple example.

Suppose candidate contact node 1 of body 1 has contacted body 2 somewhere between candidate contact nodes 1 and 2 of body 2 (see Fig. II-6). The analog of (II-4) is for the present case (we are here allowing for frictional forces):

$$\left[\begin{array}{c|c} \underset{\sim}{\alpha} & \underset{\sim}{0} \\ \hline \underset{\sim}{0} & \underset{\sim}{\alpha} \end{array}\right] \left\{\begin{array}{c} \underset{\sim}{y}_1 \\ \hline \underset{\sim}{y}_2 \end{array}\right\} \qquad \text{(II-14)}$$

where

$$\underset{\sim}{\alpha} = \begin{bmatrix} 0 & 1 & 0 & 0 \\ 1 & 0 & -(1-\alpha) & -\alpha \\ 0 & -(1-\alpha) & 0 & 0 \\ 0 & -\alpha & 0 & 0 \end{bmatrix} ,$$

$$\underset{\sim}{y}_j = \begin{Bmatrix} x^1_{j1} \\ \tau_{j1} \\ x^2_{j1} \\ x^2_{j2} \end{Bmatrix} , \quad j = 1, 2 ,$$

α is defined in Fig. II-6 and $\underset{\sim}{0}$ is the 4 x 4 zero matrix. The fictionless case can be accomodated by transforming to local normal-tangential coordinates and imposing conditions analogous to the above only in the normal direction, viz., let the subscript n and s represent the normal and tangential directions, respectively and replace (II-14) by

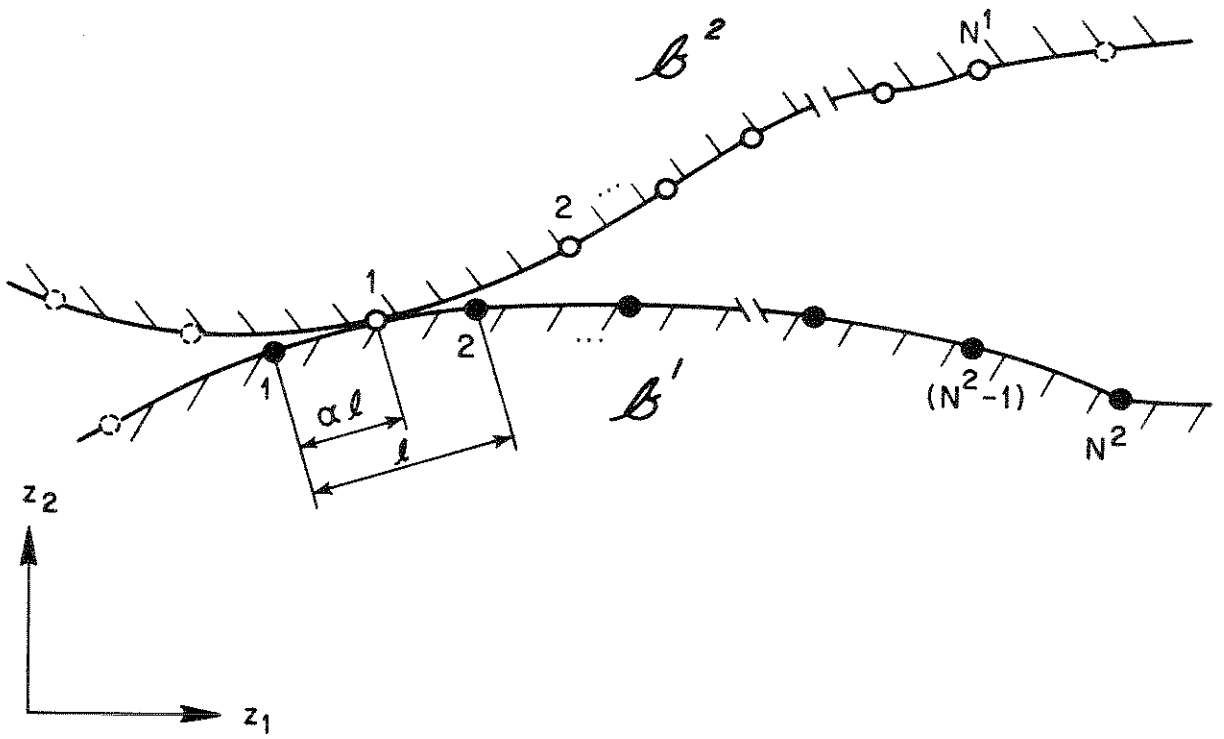

FIGURE II-6 BODIES $\mathcal{B}'$ AND $\mathcal{B}^2$ MAKING CONTACT IN THE CONFIGURATIONS $\mathcal{B}^1$ AND $\mathcal{B}^2$.

$$\begin{bmatrix} \underset{\sim}{\alpha} & \vdots & \underset{\sim}{0} \\ \cdots & \cdots & \cdots \\ \underset{\sim}{0} & \vdots & \underset{\sim}{\beta} \end{bmatrix} \begin{Bmatrix} \underset{\sim}{y}_n \\ \\ \underset{\sim}{y}_s \end{Bmatrix} \tag{II-15}$$

where

$$\underset{\sim}{\beta} = \begin{bmatrix} 0 & 0 & 0 & 0 \\ 0 & 1 & 0 & 0 \\ 0 & 0 & 0 & 0 \\ 0 & 0 & 0 & 0 \end{bmatrix}$$

and $\underset{\sim}{y}_n$ and $\underset{\sim}{y}_s$ are obtained by replacing i by n and s, in the previous definition of $\underset{\sim}{y}_i$. The matrix of (II-14) (or (II-15), in the frictionless case) is added to the global stiffness as before. On the other hand, when candidate node 1 of body 1 is <u>not</u> in contact anywhere between candidate nodes 1 and 2 of body 2, then we replace (II-14) by

$$\begin{bmatrix} \underset{\sim}{\beta} & \vdots & \underset{\sim}{0} \\ \cdots & \cdots & \cdots \\ \underset{\sim}{0} & \vdots & \underset{\sim}{\beta} \end{bmatrix} \begin{Bmatrix} \underset{\sim}{y}_1 \\ \\ \underset{\sim}{y}_2 \end{Bmatrix} \tag{II-16}$$

with $\underset{\sim}{\beta}$ as defined above. The addition of (II-16) to the global equations achieves $\tau_{11} = \tau_{21} = 0$ and no coupling is manifested between candidate node 1 of body 1 and the zone between candidate nodes 1 and 2 of body 2.

To determine when and where contact has been made in the kinematically nonlinear case, one must proceed more systematically than for the Hertzian case. For example, we must check, at each time step, whether penetration of candidate node j of body 1, $1 \leq j \leq N^1$, has occurred anywhere between candidate nodes 1 and N^2 of body 2. An algorithm for carrying out such a general check can be programmed rather simply. However, for most realistic problems

a priori geometric knowledge will probably be available and a more computationally efficient algorithm can be constructed to take advantage of this information. For example, it may be reasonable to limit the contact zone for candidate node 1 of body 1 to the zone between, say, nodes 1 to 3 for body 2. If this is the case, many less computations are necessitated. Such concepts will be even more important for the three-dimensional case in which the contact surfaces are two-dimensional, thus involving more checks.

Let us now see how the kinematically nonlinear case reduces to the Hertzian case under the appropriate circumstances. Assume $N^1 = N^2 = N$ and the initial z_1, z_2-coordinates of corresponding candidate contact nodes are aligned. Also assume that the corresponding candidate contact nodes will eventually meet to the first-order. Clearly $\underset{\sim}{A} = [a_{ij}]$ must reduce to the identity matrix $\underset{\sim}{I} = [\delta_{ij}]$ under these assumptions. Thus (II-13) (for m space dimensions) becomes:

$$\sum_{i=1}^{m} \sum_{j=1}^{N} \tau_{ij}(x_{ij}^{1} - x_{ij}^{2}) \qquad \text{(II-17)}$$

which, for m = 3, is identically (II-2).

For high-frequency, or short time results, in which the impact conditions become important, we may employ the philosophy discussed in Section 7 of [1]. In essence, this can be carried out just as in the Hertzian case (see the previous section), except, under the present circumstances, we must work in local normal-tangential coordinate systems and take account of the weighting matrix $\underset{\sim}{A} = [a_{ij}]$.

III. Modifications to Increase the Efficiency of Contact/Impact Algorithms in FEAP

Employing substructuring concepts, we have modified FEAP to increase the efficiency of the algorithm used to determine the contact region and forces. The principal modifications are to the total tangent stiffness formation scheme and to the Gauss elimination algorithm.

In solving contact/impact problems with the theory developed in [1] we originally used the algorithm shown on pages 40 to 43 of [1]. In this algorithm all matrices are evaluated for each element at each time step and/or each iteration required to complete a solution to the problem. We have noted that it is usually not necessary to use this generality except in the vicinity of the contact region. Accordingly, we have modified the programmed Hertzian contact/impact algorithm. We use the definitions of the terms given in [1] to define

$$\underset{\sim}{K}^{*} = \frac{1}{\beta \Delta t^{2}} \underset{\sim}{M} + \partial_{u} \underset{\sim}{K}$$

and

$$\underset{\sim}{R}^{*} = \underset{\sim}{R} - \underset{\sim}{K} \left(\underset{\sim}{u}_{n+1}^{(i)}; \underset{\sim}{u}_{n}, \dot{\underset{\sim}{u}}_{n}, \ddot{\underset{\sim}{u}}_{n} \right)$$

$$-M \ddot{u}_{n+1}^{(i)} .$$

Thus our solution is determined at time t_{n+1} by successively solving

$$\underset{\sim}{K}^{*} \Delta \underset{\sim}{u}^{(i)} = \underset{\sim}{R}^{*}$$

and

$$\underset{\sim}{u}_{n+1}^{(i+1)} = \underset{\sim}{u}_{n+1}^{(i)} + \Delta \underset{\sim}{u}^{(i)} \quad .$$

until $\Delta \underset{\sim}{u}^{(i)}$ satisfies equation (65) in [1].

Using the above definitions of matrices, the modified algorithm developed is shown in Table III-1. In sample computations the revised algorithm has reduced the stiffness formation times by over 75%, the equation solving times by about 50% and the resulting total computer timesby 10-40%. The lower reductions were for bar problems where the equation solution times and the stiffness form times are a small fraction of the total time. The larger savings was for a simple two-dimensional axisymmetric model (see Figure III-1 for mesh layout) and thus is more representative of the savings which can be anticipated using the modified algorithm. The breakdown of a timing record is shown in Table III-2.

The modified algorithm is essentially a scheme in which the body is subdivided into two substructures. For the first substructure (continuum elements) we form and reduce the matrix to the level of the first equation in substructure two (contact elements). We then use the resulting matrix as input to initialize the second substructure. The solution process is then completed as described in Table III-1. As is demonstrated by the results in Table III-2, this scheme results in considerable savings in the formation of stiffness matrices and in the solution of the equations by Gauss elimination.

Table III-2 also demonstrates the considerable costs involved in reporting printed results. To eleviate this cost and, at the same time, to permit more visual and selective data reporting, we have developed a graphics package for use in FEAP. Some examples of this work are included in Section I.

TABLE III-1

MODIFIED SOLUTION ALGORITHM FOR CONTACT/IMPACT ANALYSES

1. Initialize $\underset{\sim}{K}^*$ to zero, input Δt for the sequence.
2. For each time sequence in the analysis compute contributions to $\underset{\sim}{K}^*$ for each continuum finite element.
3. Determine the first equation, NPF, in $\underset{\sim}{K}^*$ which will be modified by the remaining contact elements.
4. Factor $\underset{\sim}{K}^*$ to equation NPF-1 using Gauss elimination and place the factored $\underset{\sim}{K}^*$ into backing storage.
5. For each time step and/or iteration in the sequence read the partially factored $\underset{\sim}{K}^*$ into core.
6. Initialize $\underset{\sim}{R}^*$ to the current load level $\underset{\sim}{R}$.
7. For the continuum elements compute the contribution to $\underset{\sim}{R}^*$.
8. For the contact elements determine the state of penetration and add the appropriate contributions to $\underset{\sim}{K}^*$ and $\underset{\sim}{R}^*$. This completes formation of $\underset{\sim}{K}^*$.
9. Reduce $\underset{\sim}{R}^*$, complete factoring of $\underset{\sim}{K}^*$, and back substitute to determine $\Delta\underset{\sim}{u}^{(i)}$.
10. Update solution $\underset{\sim}{u}_{n+1}^{(i)}$ and check for convergence. If convergence test is satisfied continue, otherwise repeat steps 5 to 10.
11. Output solution displacements and stresses, compute new time and complete update of displacements, velocities and accelerations.
12. For each time step in the sequence repeat steps 5 to 11.
13. For each sequence repeat steps 1 to 12.

* HERTZ CONTACT PROBLEM - MESH NB. 2 *

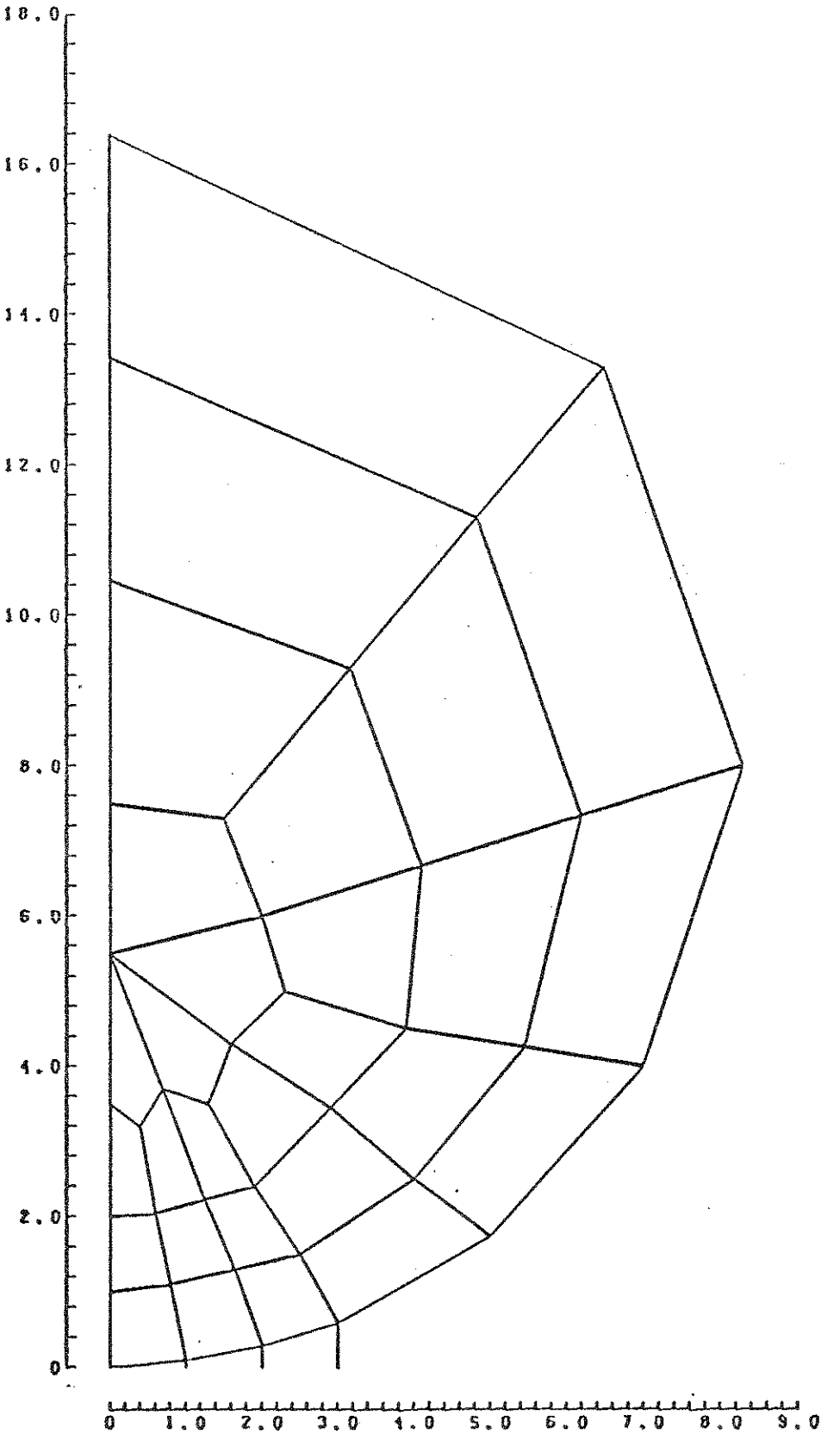

Figure III-1

TABLE III-2

SOLUTION TIME LOG FOR

IMPACT OF SPHERES PROBLEM

Item	Execution Time in Seconds	
	Original Algorithm	Modified Algorithm
1. Input of Data	0.774	.783
2. Check of Data	0.404	.408
3. Form Stiffness	36.131	7.611
4. Solve Equations	13.434	7.165
5. Output Stresses	24.682	24.654
6. Implicit Algorithm	10.602	10.084
Total Time	86.027	50.705

CONCLUSIONS

The three tasks funded under the increased effort phase of Contract No. N62399-73-C-0023 have been completed and are reported upon herein.

The veracity of the Hertzian contact/impact algorithm programmed in FEAP has been demonstrated on several test problems and the importance of the impact/release conditions has been shown. Based upon our developments we are currently able to very accurately solve difficult problems involving wave propagation.

The Hertzian contact/impact algorithm has been made much more efficient by instilling it with substructuring concepts. This has been demonstrated by numerical experiments involving typical meshes.

We have initiated the development of a methodology for incorporating the full kinematically nonlinear contact/impact problem into a finite element program. The formulation is a direct generalization of the Hertzian contact/impact scheme which is now successfully implemented. Thus we feel the kinematically nonlinear scheme proposed is highly promising and, once implemented in FEAP, will prove to be a versatile, economical tool for the solution of nonlinear contact and impact problems.

REFERENCES

1. T. J. Hughes, R. L. Taylor and J. L. Sackman, Finite Element Formulation and Solution of Contact-Impact Problems in Continuum Mechanics, SESM Report No. 74-8, University of California, Berkeley, May, 1974.

2. O. C. Zienkiewicz, The Finite Element Method in Engineering Science, McGraw-Hill, New York, 1971.

3. W. Goldsmith, Impact, Edward Arnold, London, 1960.